ELUCIDATING THE ROLE OF TRIM44 IN CANCER THROUGH RNA SEQUENCING ANALYSIS OF PRESERVED CANINE BRAIN TISSUE

A Thesis

Presented to the Faculty of the Graduate School

of Cornell University

in Partial Fulfillment of the Requirements for the Degree of

Master of Science

by

Michael Platov

August 2016

ABSTRACT

Aging is an inevitable human fate that carries with it an increasing incidence of crippling, incurable diseases such as cancer. Changes in cellular physiology that accompany the aging process are nuanced and not fully understood. Given greater insight into these processes, it follows logically that clinical interventions designed to slow aging at the cellular level will lead to a protracted incidence in diseases of aging and stand to benefit both human lifespan and healthspan.

Unfortunately, studies of these mechanisms in humans are naturally limited by ethical considerations, lack of available tissue samples from individuals of advanced age, and heterogeneity in terms of genetic background and environment that all stymie advances in aging research. We sought to use the model organism *Canis familiaris*, the domesticated dog, to circumvent these difficulties. In addition to having a shared environment with humans, *C. familiaris* has the greatest variety in body size, lifespan, and appearance of any other mammal species. At the extreme ends of the species, pint-sized, long-lived breeds such as the Chihuahua can outlive large, short-lived breeds such as the Great Dane by as much as 3-fold, while also being more resistant to certain diseases of aging. We aimed to leverage this huge difference in the rate of aging of different breeds in order to gain novel insight into the molecular workings of the aging process.

To accomplish this aim, we performed an RNA sequencing analysis of fifteen formalin-fixed, paraffin-embedded canine brains from Beagles and Boxers. Previous studies had demonstrated that Boxers (and other brachycephalic breeds) are predisposed to intercranial neoplasias, pathologies whose incidence increases with age,

while Beagles showed no enrichment for the same pathologies and also possess a slightly longer average lifespan.

Using a customized library preparation protocol and the Illumina TruSeq platform, we were able to isolate a subset of genes from our analysis whose expression correlated with age and which had functional relevance to cancer progression. Collating these data with known brain aging genes in mouse and human, the tripartite-motif containing family member TRIM44 surfaced as a candidate gene with strong correlation between expression and age, as well as the same trajectory of expression with age, in all three mammalian systems.

With known functions in neuronal maturation as well as elevation in other cancers, we questioned the role of TRIM44 on cancer growth and cell death *in vitro* using a mouse neuroblastoma line, N2A. Transient short hairpin knockdown of TRIM44 in these cells both reduced viability and promoted cellular apoptosis in response to the genotoxic stressor, etoposide. Additionally, Western blot analysis showed knockdown of TRIM44 leading to a decrease in the phosphorylation of AKT, a key signaling intermediate in the mTOR signaling pathway responsible for cell growth and resistance to cell death.

Though there are undoubtedly other factors involved in the pathology of aging and its diseases, our distillation of TRIM44 from a large RNA-seq dataset, and the subsequent functional validation of its role in cancer growth and stress resistance, seeks to highlight the statistical strength of our canine brain system. We aim to continue discovering additional factors governing aging and its disease for the improvement of human healthspan.

BIOGRAPHICAL SKETCH

Michael Platov was born in Kiev, Ukraine in 1990. He emigrated to the United States in 1995 with his mother and settled down in New Jersey with his grandparents. He attended Livingston High School, where his aptitude for the Life Sciences was first seeded and would later bloom in his tenure at Carnegie Mellon University in Pittsburgh, PA. A necromantic fixation with the study of aging brought Michael to the lab of Javier Lopez, where he was exposed to the ROS theory of aging and the effects of ETC inhibition on lifespan. Pursuing this line of research brought Michael to Cornell University, where he met Dr. Sergiy Libert and continued his journey into the aging field, albeit with a unique model system in canines.

DEDICATION

I’d like to dedicate this to everyone who kept me going through the years, those who challenged me, those who kept me up at night, and those who helped me.

It was a privilege to spend my time at Cornell with you all.

ACKNOWLEDGEMENTS

I’d like to firstly acknowledge my mentor, Dr. Sergiy Libert, without whom none of this would be possible, as well as all the members, past and present, of the Libert Lab.

Funding for this project came partly from a stipend from a 2015 AFAR Research Grant for Junior Faculty.

TABLE OF CONTENTS

Background and Significance

A multitude of pathologies including cancer, type II diabetes, and neurodegenerative disease such as Alzheimer's disease and ALS, share aging as a common risk factor [1]. Indeed, while palliative care for these conditions improves, there is as of yet no "cure" for these diseases of aging. Given aging as a common risk factor, it follows that interventions that slow down aging will also decrease the propensity of aging-related diseases and lead to an increase in both human lifespan and healthspan.

The definition, mechanism, and even inevitability of aging are topics that are still in debate. Several "wear-and-tear" theories exist for why age-associated decline occurs at the cellular level, not limited to stem cell depletion [2][3], buildup of intracellular damage due to reactive oxygen species (ROS) [4], and loss of replicative fidelity as a consequence of DNA damage and mutation [4][5]. By this logic, organisms with longer lifespans have evolved more sophisticated repair mechanisms to combat this progressive decline, whether in the form of better individual repair mechanisms, ex. greater accuracy of DNA repair, or better systematic sensing of/response to environmental insult. As an example of the latter point, the long-lived naked mole rat has been revealed to have a mutant version of the pivotal tumor-suppressor protein, p53, which is weaker at stimulating hypoxia-mediated apoptosis, yet naked mole rat cells rarely become cancerous due to a systemic upregulation of necrosis in response to aberrant cell function [6][7].

A separate school of thought in the aging field, that of "programmed aging", posits that cells inevitably undergo programmed cell death, or apoptosis, as a method of removing old, defective cells and preserve the healthy cells around them [8][9]. Indeed,

this process is observed at many levels including the level of the cell (apoptosis), the organelle (ex. mitoptosis), and the organ (organoptosis) [10]. Extensions of the idea of "programmed aging" include the concept of the Hayflick limit, a fixed number of mitotic divisions past which point cells lose the ability to divide due to telomere shortening and either undergo apoptosis or senescence [11] . Since this concept does not work in largely post-mitotic aging models, such as the nematode *C. elegans*, another concept of "programmed aging" suggests a hyperfunction/hypertrophy model wherein developmental and growth programs initiated early in life, programs that maximize reproduction, continue to function later in life at the expense of organismal fitness. Continued activation of oncogenic cell processes, namely the Ras and TOR signaling pathways, accelerates the rate at which cells reach terminal senescence [12]. As an analogy, you can equate this to turning the faucet to fill a bath (early life), but leaving the faucet on (late life) and causing the bath to overflow. Similar to this is the "disposable soma theory", the idea that organisms have evolved in such a way as to maximize organismal fitness, which is defined as the number of surviving offspring produced [13]. To that end, evolution has selected for those traits that benefit early life reproduction at the cost of survival and the fitness later in life. Such a theory explains how Huntington's disease's, for example, has persisted in the population despite being autosomal dominant and lethal – it's age of onset, between 35 and 45 years, is past the point of peak reproductive performance and thus has not been under negative selective pressure, while the huntingtin mutation itself increases fecundity and many reduce early cancer risk [14]. In more practical applications, DNA methylation levels have been shown to be predictive of age – Horvath's clock, a collection of 353 epigenetic markers

on the genome, can be used to accurately estimate the chronological age of a tissue based on its methylation status [15], though it is unclear whether these markers specifically have a function in aging or reflect the declining quality of epigenetic control with age.

Regardless of the actual mechanism governing cellular aging, several metabolic pathways are known to impact the *rate* of cellular aging. The following is a brief description of the these main pathways and their mechanisms of action:

a) **The FOXO3/Sirtuin pathway**

FOXO3 is a member of the forkhead family of transcription factors and variants have been linked to longevity in numerous cohort studies [16]. FOXO3 has been suggested to induce pro-apoptotic programs, autophagy and mitophagy, DNA repair, and overall lead to increased lifespan by protecting from age-related diseases such as cancer and neurodegenerative disease [17]. Sirtuins are a class of NAD^+-dependent deacylases with broad cellular function and localization [18]. Deacetylation of FOXO3 by SIRT1 has been shown to attenuate FOXO3-mediated cell death, instead promoting cell stress resistance pathways, lipid metabolism, and gluconeogenesis as an adaptation to conditions of low nutrient intake [19]. Caloric restriction (CR), a dietary program whereby starvation-like conditions are induced while maintaining minimum nutrient requirements, has been hypothesized to act as a mechanism to activate SIRT1 activity, whether by increasing synthesis of NAD^+ or upregulating NADH hydrogenase activity [20]. An interesting caveat is that caloric restriction in mice was shown to *decrease* SIRT1 activity in the liver despite increasing it in other metabolically-active tissues, such as white adipose tissue and muscle – this is thought to occur because the liver is the

hub of fat and cholesterol synthesis, processes which require NAD to be reduced and favor energy storage rather than entry of NADH into electron transport. Caloric restriction has been shown to increase lifespan in a number of mammals including mice, dogs (Labrador Retrievers), and even primates [21][22][23], though there is controversy surrounding the latter observation. To illustrate this controversy, a 20-year longitudinal study published in 2009 from the University of Wisconsin-Madison showed numerous longevity-promoting phenotypes in rhesus macaques with adult-onset CR, not limited to reduced incidence of diabetes, cancer, cardiovascular disease and brain atrophy [24]. Conversely, a 23-year-long study performed at the National Institute on Aging (NIA) and published in 2012 found no statistically significant difference in survival between control and calorically restricted groups, regardless of whether CR was initiated in adulthood or youth, though other parameters, such as delay of onset of age-associated disease, *did* match the observations of the 2009 study [25]. Finally, a 2014 follow-up to the 2009 study reiterated a CR-based extension of longevity in rhesus macaques [26], citing the differences in diets between the macaques used in the 2009 and 2012 studies as confounding to the results – the NIA study used feeding regiments instead of a true *ad libitum* diet, which could have been enough to simulate some CR phenotypes as caloric restrictions as little as 10% has been shown to increase lifespan in other mammalian models [27]. Within the realm of pharmaceutical application, Resveratrol, a caloric restriction mimetic, has also been shown to increase lifespan in flies, fish, and mice fed a high-fat diet, with trials in dog set to begin shortly [28][29]. Certain SIRT1 activators were also found to have a similar positive effect on lifespan through repression of pro-

inflammatory NF-kB and cytokine signaling [30].

b) **The growth hormone/IGF-1 signaling pathway**

Growth hormone signaling promotes organismal growth and development, activating several anabolic cellular signaling cascades including the MAPK-ERK and JAK-STAT pathways, the latter of which produces the endocrine hormone IGF-1 [31][32]. IGF-1 in turn is a strong agonist for the mTOR/AKT signaling pathway, which stimulates cellular proliferation and inhibits apoptosis. IGF-1 has been documented as having a predictive effect on organismal size in dogs [33]. Parallel to this, mutations that lead to deficits in IGF-1 production or reception lead to clinical dwarfism, while defects in the anterior pituitary that illicit growth hormone overproduction lead to gigantism [34]. In worms, daf-2 (the homolog to mammalian IGF-1 receptor) mutants have been shown to have dramatically increased lifespan [35]. Snell dwarf and Ames dwarf mice, two lines that simultaneously lack growth hormone, prolactin, and thyroid-stimulating hormone, have both been shown to have significant lifespan extension compared to non-dwarf littermates when grown in protective conditions [36]. The same lifespan extension is not seen in human dwarves, though patients with Laron syndrome (dwarfism due to lack of growth hormone receptors) have much lower risk of cancer and diabetes, two prominent diseases of aging [37]. DNA damage can act as a suppressor of IGF-1 signaling: nucleotide excision repair (NER) deficient mice, despite having shortened lifespans, have been shown to have reduced serum IGF-1 levels paired with cell-protective phenotypes such as reduced oxidative metabolism and increased anti-oxidant defenses associated with reduced IGF-1 signaling [38]. Oppositely, IGF-1 supplementation and small molecule upregulation have been pursued for treatment of

ALS, albeit with mixed results [39]. Connecting the caloric restriction pathway with IGF-1 signaling, long-lived growth hormone receptor knockout mice (GHRKO) showed elevated FOXO1 protein levels and SOD2 expression, concomitant with a role for elevated expression of FOXO family proteins in longevity and reduction of ROS levels [40]. However, these mice did not show elevated SIRT1 expression, suggesting that IGF-1 signaling and caloric restriction work through similar (i.e. FOXO regulation) yet divergent pathways.

c) **Activity of the mitochondrial electron transport chain**

Oxidative phosphorylation results in the production of ATP from ingested macromolecules, with oxygen acting as the terminal electron acceptor in the electron transport chain (ETC) to produce H_2O. With age, numerous changes occur to mitochondrial function including reduction in clearance of damaged mitochondria, decrease in mitochondrial biogenesis, and decline in mitochondrial quality control, all contributing to decreased respiration and ATP production [41]. In terms of "wear-and-tear", the process of mitochondrial respiration is naturally inefficient and prone to electron leakage most prominently at Complex I and Complex III of the ETC, the byproduct of which is superoxide radicals that are further reduced to hydrogen peroxide [42]. These superoxide radicals, in turn, adversely affect numerous cellular functions, primarily promoting formation of DNA lesions [43]. Catalases and superoxide dismutases (SOD) counteract these radicals but are not perfectly efficient, leading to gradual buildup of damaging intracellular ROS. In relation to aging, SOD knockout animals show decreased lifespans, and buildup of intracellular ROS and inflammation have been associated with ALS [44]. Conversely, flies and worms defective in ETC

function have both decreased respiration and increased lifespan [45], though this observation casts skepticism on the wear-and-tear ROS theory of aging given that these mutants have paradoxically *increased* ROS. Studies have suggested a daf-16/FOXO-mediated mode of action for this longevity mechanism, where increased ROS acts as a signaling molecule to promote nuclear translocation of the daf-16/FOXO transcription factor through JNK reception, leading to expression of pro-longevity genes [46]. In a similar vein, chemically-induced glucose restriction in worms has also been shown to increase mitochondrial function and oxidative stress, culminating in AAK-2 dependent lifespan extension [47]. Interestingly, this result was abolished by pre-treating the worms with antioxidants; the authors suggest that these findings support a “mitohormesis” model wherein small, non-lethal doses of mitochondrial stress prime the cell to further stress, inducing cell-protective mechanisms that promote longevity. On the other hand., ROS signaling has been shown to promote growth through mTOR signaling, as well as promote HIF1 (hypoxia-inducible factor) activation, processes which normally *inhibit* FOXO signaling [48]. Yet another study suggests that the transcription factor Nrf2 is responsible for ROS-mediated longevity increase, showing the gene to be activated by caloric restriction and Nrf2 signaling being elevated in the long-lived naked mole rat [49].

Despite this breadth of knowledge regarding the metabolic processes that may play a hand in physiological aging, the above methods suffer from a number of limitations that hamper their direct applicability to the improvement of human healthspan, in addition to the debate over the exact molecular mechanism by which some of these longevity-increasing strategies operate. For instance, it is hard to apply a

strategy such as caloric restriction to improve human lifespan because in research models it is reported to only be effective when started relatively early in life, is uncomfortable in practical terms, and comes with adverse secondary effects such as loss of bone density and muscle mass [50]. Additionally, given that many of these pathways were studied in lower vertebrates or invertebrates such as *C. elegans*, their direct applicability to humans is in question. This fact is confounded further by the difficulty of gene modulation *in vivo*, as well as the variable efficacy of drugs designed to mimic these effects (ex. resveratrol) [51].

Comparative, high-throughput aging studies both across and within a species have been another avenue taken to explore the dynamics of aging, and have contributed greatly to our mechanistic understanding of the aging process. The Gorbunova group at the University of Rochester has a collection of over 30 different fibroblast lines from various members of the order Rodentia, spanning lifespans as short as 4 years to as long as 32 years, including the famously cancer-resistant naked mole rat. The study found somatic telomerase activity in rodent tissues was inversely correlated with the log body mass, not lifespan, of the donor species, an observation that suggests that a greater raw cell count in larger organisms triggered an evolutionary shift towards increased anti-tumor mechanisms, including telomerase repression and replicative senescence, in their somatic cells [52].At the same time, this result draws attention away from the importance of telomere length as a predictor of longevity – as an example, lab mouse strains, despite having telomeres over 5-fold longer than humans, as well as somatic telomerase expression, have a nearly 30-fold shorter average lifespan [53]. In a sister study by the Vijg group, DNA repair in livers of 3

species, naked mole rat, human, and mouse, was found to correlate positively with species lifespan in terms of expression of key genes in the double-strand break repair pathway, including TP53, NHEJ1, and polymerase λ [54]. Concurrently to the rodent study, the Gladyshev group is performing a much broader study that incorporates mammals from vastly different phylogenetic families, including the extremely long-lived bowhead whale as well as Brandt's bat [55][56]. Relatedly, a study by the de Magalhaes group was able to identify groups of genes that underwent positive selection in tandem with evolution events that increased species longevity, which include the proteasome-ubiquitin system and DNA repair genes such as DDB1 and CAPNS1 [57]. Yousin Suh at the Albert Einstein College of Medicine has sequenced genomes of over 400 centenarians of Ashkenazi Jew descent, confirming both IGF-1 signaling and telomere length to be conserved longevity-assuring pathways [58][59]. A related vein of study in American descendants of Okinawan centenarians, spearheaded by the Willcox twins at the University of Hawaii, has found extensive connections between FOXO, mTOR signaling, and aging [60].

Recent reviews have also suggested the use of alternate mammalian systems with which to better elucidate the trajectory and mechanisms of aging. Studies of longevity in humans have naturally been set back by ethical considerations, difficulty of obtaining large sample sizes of patients of advanced age, and large potential variation in environment and background. Lab mice have become an indispensable tool for analyzing the effects of gene modulation in a mammalian background now more so than ever due to the advent of CRISPr/Cas9 technology, especially in the context of development and stem cell therapy. In general, however, the number of genetic

backgrounds available for use are limited, and between these backgrounds there is very limited variation within average lifespan, which bars any meaningful longitudinal study of aging [61]. In addition, findings in mice and other rodents are not always applicable to humans, despite similarities in our physiology. As a solution to these pitfalls, enter *Canis lupus familiaris*, the domesticated dog.

C. familiaris has emerged as an excellent model organism to study human aging for a number of reasons. Phylogenetic evidence suggests that the original wolf ancestor of the modern domesticated dog is now extinct, making it difficult to accurately pinpoint when domesticated dogs arose [62]. However, DNA sequencing indicates grey wolves as a recent ancestor as determined by similarity in mitochondrial cytochrome B sequence, with the two species diverging up to 40,000 years ago. Multiple lines of evidence support the idea of canid and human co-evolution. Increased copy number of salivary amylase AMY2B in dogs compared to wolves suggests an adaptation to increased starch consumption in agricultural refuse in tandem with the transition of humans from hunter-gatherers to an agricultural society [63]. This adaptation is matched by increased positive selection at the SGLT1 locus, which encodes an intestinal glucose/sodium transporter required for downstream starch metabolism. Relatedly, the MGAM gene coding for a maltase-glucoamylase required for starch digestion and the cholesterol transporters ABCG5 and ABCG8 show evidence of strong positive selection in dogs when compared to wolves, supportive of a shift towards an omnivorous diet. Interestingly, these genes show a similar trend for positive selection in humans, further supporting a co-evolution model [64][65]. Genes associated with behavior, neural plasticity, and aggression also show positive selection in domesticated

dogs [66]. Interestingly, the other most represented category of genes under parallel positive selection in both domesticated dogs and humans, besides those associated with metabolism and behavior, are cancer and cell death-related genes, such as MET (met proto-oncogene) and BFAR (bifunctional apoptosis regulator) [66]. Indeed, the age of onset and vulnerabilities to specific types of cancer are quite similar between dogs and humans, eg. intercranial neoplasias (**Figure 1**). In addition, aged dogs share Alzheimer's disease symptoms with humans including loss of brain volume and impairment of both neural stem cell quantity and function at the dentate gyrus [67].

One of the greatest strengths of the canine system is the observation that within its species, *C. familiaris* has unprecedented diversity in terms of average lifespan, size and weight per breed. The trend of average lifespan in relation to average weight for all American Kennel Club-recognized breeds, as well as the lifespan distribution of these breeds, highlights this diversity - note the almost 3-fold difference in average lifespan between the shortest and longest-lived breeds (6 years – Irish Wolfhound, 17 years – Chihuahua) (**Figure 2A, B**). IGF-1 has previously been linked to the difference in size in breeds in a seminal NIH study. Given the connection between IGF-1 signaling, growth, and aging, it has been proposed that large, shorter-lived breeds do in fact *age faster* than their smaller, longer-lived counterparts [68], a phenomenon recapitulated in other mammalian models such as the long-lived Brandt's bat and the long-lived Snell mouse. Indeed in most mammalian species, though there is a trend towards larger species having longer lifespans, the opposite holds true *within* a species – smaller members of a species tend to live longer [69]. Though there are undoubtedly other factors governing the observed lifespan differences between breeds other than the IGF-1 axis, there is

unprecedented analytical power in a comparative study of canines. Taking the example of the Irish Wolfhound and Chihuahua, if the Wolfhound ages 3-times as quickly as the Chihuahua then it follows that transcriptional and proteomic changes that occur with aging will be much more pronounced when comparing members of these two breeds than when comparing two aged humans, given a relatively homogenous average human life expectancy of ~80 years in developed countries.

The work that will be presented in this thesis sought to utilize the power of the aforementioned dog model in order to discover novel longevity determinants. Capitalizing on a large available collection of preserved canine brain samples through a collaborator at the Cornell University College of Veterinary Medicine, we interrogated the age-associated gene expression changes of 15 canine brains spanning a 1 to 11 year age range using high-through RNA sequencing on the Illumina platform. With this data, it is our intent to demonstrate both the power of this relatively unexplored model as well as its significance to the improvement of human health.

Materials and Methods

RNA isolation and purification from FFPE samples

RNA was extracted from formalin-fixed, paraffin-embedded sections normalized to the cerebral cortex of dogs that had been hospitalized and euthanized by the Cornell University Hospital for Animals. Reasons for hospitalization varied – a sample pathology report is included at the end of this document. FFPE sections used for RNA extraction were ensured to not be from pathological tissue, and sections were normalization to the same region of the brain, the cerebral cortex, using hematoxylin and eosin (H&E) staining (**Supplementary Figure 1**).

For each brain two 15µm histological scrolls were cut from each paraffin block. The scrolls were stored at -80 degrees C or shipped on dry ice to another facility for purification. Both in-house and at the second facility, RNA was purified using the Agencourt FormaPure kit (Beckman Coulter). Samples were heated in buffer to release the tissue from paraffin and to reverse crosslinking. Total nucleic acids were freed from the tissue by protease K digestion. Samples were transferred to a BioMek 4000 Automated Liquid Handling System (Beckman Coulter). The Automated System binds nucleic acids to carboxyl-coated magnetic beads, immobilizes the bead-bound nucleic acids using a magnet provided with the system, treats the samples with DNase to remove genomic DNA, and then washes with alcohol solutions. Modifications to the standard protocol included using 85% ethanol (to include small RNAs) followed by an isopropanol wash (to counteract the fatty nature of the nervous tissue). RNA was eluted off the beads using nuclease free water. The concentration and purity of the samples

was assessed by spectrophotometry (Nanodrop) and RNA integrity was quantified on a Fragment Analyzer (Advanced Analytical).

To further improve library quality, total RNA was depleted of ribosomal RNA (rRNA) using the Ribo-Zero Magnetic Gold Kit (Human/Mouse/Rat)(Illumina). Sequencing library preparation was subsequently performed using the Illumina TruSeq® RNA Library Preparation Kit v2. The fragmentation step of this sample was skipped because RNA from FFPE samples had been previously reported to *already* be heavily fragmented due to the cross-linking process [70]. SuperScript II® Reverse Transcriptase (Invitrogen) was used to synthesize the cDNA libraries using Illumina sequencing indexes. Sample quality was tested at two timepoints using an Agilent 2100 BioAnalyzer: 1) Before rRNA-depletion and 2) immediately after final library preparation. Representative images of these quality checks are included (**Supplementary Figure 2**).

Library preparation, sequencing and analysis

Libraries were sequenced on the Illumina HiSeq 2500 platform with single-end 100bp reads, with a pass filter output of 22-25Gbp per lane. A total of 15 libraries were sequenced, multiplexed as 7 and 8 samples across 2 wells. The average raw read mass across all samples was 5.8M, with an average mapping rate of roughly 98.5% to the whole genome of the CanFam3.1 canine genome assembly and a 4.7% average mapping rate to the transcriptome alone at a 24.7% multiple alignment rate.

Analysis of the sequencing data was performed using a protocol adapted from Dr. Jen Grenier at Cornell University using the Tuxedo Suite of RNA-seq analysis software. In brief summary, FastQC was used to filter out reads below 100bp while cleaving off

index primer sequences from these reads, Tophat was used to build a transcriptome index from the CanFam3.1 genome assembly (Broad Institute) and map the trimmed reads to this index, Cuffquant was used to quantify and normalize gene expression from the Tophat-generated BAM files, and Cuffdiff was used to convert Cuffquant-generated CXB abundance files to a usable Excel format. Mapping stringency was reduced for this study by increasing mismatch tolerance in order to accommodate the increased number of mutations introduced by the fixation process [70]. Further post-processing and analysis, including principal component analysis and log transformation, was performed using R programming software.

N2A cell maintenance and Cell growth assay

Neuro-2a (N2A) cells were grown in standard growth medium with 10% fetal bovine serum and Pen Strep (Thermo Fisher). Cells were seeded at a density of $0.2x10^5$ cells per well in a 6-well culture plate and transfected 24 hours later with one of five mTRIM44 shRNA plasmids (OriGene, TL512542), a control shRNA plasmid, or no plasmid at all using the FuGENE® HD Transfection Reagent (Promega). A 1-to-7 ratio of µg plasmid to µL FuGENE reagent was used for all transfected conditions and controls. Cells were imaged at the same timepoint for 4 subsequent days using a Zeiss inverted microscope and the AxioVision 4.8 imaging suite. Images were collected using the MosaiX tool programmed to take a representative collage of 35 images (5 rows x 7 columns) per sample. Cell counts were computed from these images using ImageJ software (‘AutoThresholdAndSegment’ macro by Gilles Carpentier, Université Paris).

Quantitative PCR

RNA was collected from transfected N2A cells grown as described above using the TRIzol® reagent (Thermo Fisher). Synthesis of cDNA was performed using the SuperScript® III Reverse Transcriptase system (Thermo Fisher). Quantitative PCR was carried out using Maxima SYBR Green (Thermo Fisher) at the recommended cycling conditions on a Bio-Rad CFX96 Touch™ Real-Time PCR Detection System. Expression values were calculated in terms of ΔCq relative to ActinB and, unless stated otherwise, were run in triplicates.

Primers used:

ActinB	R: CTG ATC CAC ATC TGC TGG AAG GT
	F: GAC AGG ATG CAG AAG GAG ATC A
TRIM44 (mouse)	R: CTC TTG AAC TTT AAC CTT TCC ACC
	F: GCT CAT CTG TGT CCT GTG TC

Apoptosis assay and Flow cytometry

N2A cells were seeded at a density of $0.5x10^5$ cells per well in a 6-well culture plate. Cells were transfected 48 hours later using the same conditions as above. Transfection efficiency was assessed via quantification of eGFP fluorescence 48hr post-transfection (**Supplementary Figure 4**), at which point cells were washed and treated with 100uM of etoposide for 24 hours. Following stress treatment, cells were co-stained using a combination of LIVE/DEAD® Fixable Violet Dead Cell Stain Kit (Thermo Fisher) and Annexin V, Alexa Fluor® 647 conjugate (Thermo Fisher) to test for cells in late and early apoptosis, respectively. Flow cytometry was subsequently performed on a BD FACSAria III with a threshold of 10,000 gated events per sample. Cells that did not stain

for at least one of the two dyes (fluorescence signal of “0”) were barred from further analysis.

Western blotting

Cellular protein content was extracted from lysis of confluent N2A cells using RIPA buffer supplemented with protease inhibitors. Protein concentrations were quantified using the Bradford reagent at A595 and final protein concentrations were inferred from a sigmoidal standard curve. Samples were denatured at 95°C in Laemmlli buffer and loaded on a denaturing 13% acrylamide gel at 20ng per sample. The samples tested were 4 separate TRIM44 shRNA treatments and an shRNA control. Membranes were blotted for B-actin (42 kDa), p-Akt (Thr308) (60 kDa), Akt (60 kDa), and Caspase3 (17, 19, 35 kDA) (Cell Signaling Technology ® products) overnight at 4°C with a stripping step in between Akt and p-Akt blotting. HRP-conjugated secondary antibodies were used for blot development with Pierce™ ECL Western Blotting Substrate (Thermo Fisher). Relative protein abundance was computed relative to B-actin using ImageJ software.

Results

To assess age-based changes in gene expression in canines, formalin-fixed, paraffin-embedded brain tissue samples were selected from 15 dogs, 7 Beagles and 8 Boxers, with a wide range of donor ages (**Table 1**). Brain tissue was selected for four primary reasons:

1) Numerous, incurable diseases of aging originate in the brain, including Parkinson's and Alzheimer's disease as well as various types of cancers.

2) It is easy to normalize across a specific brain region for all our tissue samples, in this case the cerebral cortex (**Supplementary Figure 1**).

3) Brain tissue, specifically the cortical regions used in this study, maintains a relatively stable cell composition with age [71].

4) Beagles and Boxers have vastly different predispositions to intercranial neoplasias, such as gliomas [72].

For the purposes of this study, sample gender and status (spayed/castrated) were ignored. Raw sequencing data was mapped to the CanFam3.1 genome assembly using the Tuxedo Suite, with read mismatch stringency loosened in order to account for mutations introduced through the FFPE fixing process.

Within our expression dataset, we observed a high degree of reproducibility between samples (**Figure 3**), with only a few genes having a significant expression change between similarly-aged samples – we would expect most genes to remain at a stable level of expression in such a short timeframe. Interestingly, principal component analysis of our dataset showed strong clustering across sample age but not between breed (**Figure 4**), implying that there was a subset of factors in our expression dataset

that were predictive of sample age. This finding was very interesting given the documented similarity between human aging and dog aging. Extracting those genes with strong linear correlations ($R^2 > 0.5$, simple linear regression model) of expression relative to brain donor age, we also found that these genes were significantly enriched for gene ontology (GO) categories tied to age-based decline, most prominently cancer (**Supplementary Figure 3**). This observation gave us additional confidence in our dataset as it confirmed that we were in fact looking at genes that, broadly, had functions in aging-related processes and could potentially be applied to aging therapies. Moreover, the overrepresentation of cancer-related genes matched the known observation of Boxers and other brachycephalic breeds being highly prone to intercranial neoplasias, with Beagles being relatively protected from the same pathologies [72]. Though our PCA analysis did not support clustering by breed within our dataset, it was nonetheless possible that this functionally-enriched ontological group of cancer-related genes contained the factor(s) accounting for differences in cancer susceptibility between Boxers and Beagles, warranting further study of its constituent genes.

To further narrow our analysis, we sought to take advantage of mammalian homology to see if any of the genes in our dataset had already been studied in other mammalian models or otherwise linked to aging or cancer. Collating our expression data with that of the BrainCloud human brain aging dataset (GEO accession number: GSE30272) and the AGEMAP (Atlas of Gene Expression in Mouse Aging Project) mouse cerebral cortex gene expression database [73], we were able to extract a small subset of genes that a) have similar expression trends with age across all three species,

and b) have a statistically significant (P<0.1) slope as calculated by the Student's t-test (**Table 2**). Again, highlighting the strength of the canine model of aging, it was interesting to note that between the human-dog and human-mouse dataset pairings, the human-dog comparison had a higher correlation than human-mouse (measured as a Pearson correlation, not shown), demonstrating that age-associated gene expression changes between human and dogs are indeed similar and potentially more therapeutically relevant.

Out of the candidate genes that were extracted using this method, TRIM44 stood out as an especially attractive cancer-related gene due to implied function in differentiation and maturation of neuronal cells [74], as well as having a putative interaction with p53 and molecules in the Akt signaling pathway [75]. TRIM44 is a member of the tripartite motif-containing family of proteins, a group of proteins characterized by a RING finger domain, B-box zinc finger, and coiled coil motif at the N-terminus. These molecules have implications in a broad range of cellular functions including pathogen recognition and cell compartment identification, as well as ubiquitinylation function through their interaction of the conserved RING domain with E2 ubiquitin ligases [76]. Additionally, TRIM44 has previously been shown to be elevated in esophago-gastric and breast cancers, hinting at TRIM44 ablation as a potential therapeutic option for cancers [77]. The same study demonstrated co-localizion of TRIM44 with p-mTOR in patient-derived samples as well as induction of cell death upon addition of an mTOR inhibitor, everolimus, suggesting that mTOR is necessary for TRIM44-mediated cancer growth. Though these studies implied a connection between TRIM44 and cancer, they only did so in a select few cell lines, did not investigate a link

between TRIM44 and cell proliferation outside of cancer, and also did not investigate mechanisms of action outside of the mTOR pathway, which encouraged us to explore this gene in more detail.

As stated earlier, TRIM44 shares homology across most mammalian species, including human and dog. TRIM44 expression increased with age in all three mammalian datasets; pairing this result with its implied function in the mTOR/Akt pathway and neuronal differentiation supported a hyperfunction/hypertrophy mechanism of cancer promotion wherein TRIM44 activity is beneficial to maturation in early life but can cause cancer and other cellular malfunctions when overstimulated later in life. To test this hypothesis, as well as verify the molecular interplay between TRIM44 and mTOR signaling, we employed a cell culture model to test whether TRIM44 is exerting a cell-autonomous growth effect through mTOR. Given the lack of available antibodies against canine proteins, Neuro-2A (N2A) cells, a mouse-derived glioblastoma line, were used to directly assess the impact of TRIM44 modulation on cancer cells and the mTOR pathway. As expected based on literature tying TRIM44 and cancer growth, N2A cells with transient knockdown of TRIM44 (**Figure 5A**) showed decreased viability to the control shRNA treatment (**Figure 5B**), given a high transfection efficiency and robust shRNA expression at 2 days post-transfection (**Supplementary Figure 4**). All transfected samples experienced some degree of cell death following shRNA transfection likely as a side-effect of toxicity associated with the transfection reagent. In addition to growth defects, protein-level analysis showed decreased levels of p-Akt and Akt relative to B-actin in the TRIM44 shRNA-treated cells, as well as a reduced p-Akt/Akt ratio in these cells (**Figure 6A-D**), supporting that TRIM44 signaling and the

mTOR/Akt pathways are connected. Though this does not prove that mTOR/Akt inhibition is *directly* responsible for the observed decrease in cell viability, it is in line with previous observations regarding the effects of TRIM44 modulation on cancer cell growth.

Though these data supported a mechanism of TRIM44 through the mTOR/Akt pathway, it was curious to see what other downstream effects TRIM44 modulation had on the cellular environment. Outside of its function in promoting glucose uptake and protein synthesis, upregulated Akt signaling is associated with inhibition of apoptosis through suppression of p21-mediated growth arrest [78], caspase activity, and transcriptional regulators of apoptotic programs such as FOXO3 [79]. It follows logically that TRIM44 knockout would sensitize cells to apoptosis, in addition to negatively impacting cellular proliferation through inhibition of the mTOR/Akt signaling pathway. To test this, N2A cells transfected with TRIM44 shRNA constructs were treated for 24 hours with etoposide, a chemotherapy drug that inhibits DNA synthesis, to test their response to cellular stress under TRIM44 knockdown. We have previously shown that after 24hr stress with 100uM etoposide there is a visible cell death phenotype in our N2A cell line (**Supplementary Figure 5**). Cells were stained post-stress with a fluorescent Annexin-V conjugate and LIVE/DEAD® Fixable stain (Thermo Fisher) to measure the number of cells in early and late apoptosis, respectively. Following the stress treatment, there was a clear decrease in the number of surviving cells in two TRIM44 knockdown samples compared to the control shRNA-treated sample (**Figure 7A-C**), indicative of more cells in late apoptosis. The shift in Annexin-V staining was less pronounced, though in all stressed conditions there was a rightward shift towards a

larger number of cells in early apoptosis. Interestingly, the control shRNA-treated cells had a larger increase in early apoptotic cells between stressed and unstressed conditions than either of the TRIM44 shRNA-treated samples (**Table 3**). These results could indicate that under the same stress conditions, control shRNA-treated cells are more resistant and primarily express markers of *early* apoptosis, including the flipping of phosphotidylserines in the cell membrane, while N2A cells with TRIM44 knocked down are more sensitive to the stress and reach terminal apoptosis, characterized by breakdown and permeation of the cell membrane. The differences in late apoptotic staining between TRIM44 knockdown cells and the control provide further support for a mechanism of action for TRIM44 involving the mTOR/Akt pathway, possibly mediated through lack of inhibition of p21- or caspase-mediated cell death.

Discussion

To gain novel insight into the molecular mechanisms of aging we performed a high-throughput RNA sequencing analysis of over a dozen formalin-fixed, paraffin-embedded (FFPE) dog brains from donors of various age in order to discover novel genes and pathways involved in aging and its diseases. Despite the generally poor quality of FFPE samples, we were able to successfully extract high-quality RNA from our samples and map them to the CanFam3.1 genome assembly, with high reproducibility between samples (**Figure 3**). Indeed, a principle component analysis of the expression data highlighted that there was age-based clustering in our dataset, which suggested that the expression of a certain subset of “age-marker” genes was both responsible and predictive of the age of a given sample (**Figure 4**). Attempting to isolate and characterize these age markers, a gene ontology analysis was performed on the genes with the best linear fit of expression relative to age. Surprisingly, these genes were overwhelmingly enriched for genes involved in cancer (**Supplementary Figure 3**). This result prompted us to look deeper into the genes in this ontology group as Boxers and Beagles, the two breeds used in our analysis, have a stark difference in brain cancer susceptibility, and it was highly possible that we were looking at the genes responsible for this difference within our RNA-seq dataset.

Through several filtering steps applied to the raw expression data, a candidate set of genes was obtained that had a conserved, age-related trajectory of expression across humans, mice, and canine datasets (**Table 2**). This set was further narrowed down to a single gene of interest, TRIM44, a member of the tripartite motif-containing protein family. A relatively understudied group of molecules, the TRIM family proteins

contain a RING domain that associates with the E2 ubiquitin ligase machinery, but otherwise has a myriad of intracellular functions. We interrogated TRIM44 due to its putative function in neural maturation, as well as the observation that TRIM44 contributes to mTOR/Akt-dependent cell proliferation in a subset of human cancers. These observations supported a role for TRIM44 in a hypertrophy model of aging, wherein the stem cell proliferation and growth that TRIM44 promotes in early life proves deleterious in later life, where it potentially promotes cancer.

To test the hypothesis that TRIM44 is necessary for mTOR-dependent cancer growth, we phenotyped the cellular changes that occur following TRIM44 knockdown using Neuro-2a (N2A) mice neuroblastoma cells transfected with mTRIM44 shRNA constructs. The results of these experiments strongly supported a role for TRIM44 in cell proliferation. TRIM44 knockdown cells showed both decreased viability (**Figure 5B**) and decreased p-Akt signaling (**Figure 6B-D**) relative to the scramble shRNA control, validating a previous study that had shown TRIM44 to act as an mTOR/Akt pathway agonist in a subset of cancers, though we did not show that the mTOR/Akt pathway is the *only* mechanism of action by which TRIM44 knockdown impedes growth.

Further support for a mTOR/Akt mechanism of action for TRIM44 came from a stress assay designed to simulate age-associated damage – TRIM44 knockdown cells treated overnight with the DNA damage agent etoposide showed a significant increase in late apoptotic cells compared to a control shRNA sample (**Figure 7A-C**). As the mTOR/Akt pathway is normally responsible for inhibiting downstream apoptotic signaling through inhibition of caspase, FOXO proteins, and p21-mediated cell death,

this result fits with a model wherein TRIM44 knockdown and subsequent inhibition of mTOR/Akt activity leads to a disinhibition of apoptotic programs.

Addtional investigation is required in order to cement the role of TRIM44 in the aging dog brain and its applicability to human gerontology. Though we have tentatively suggested an mTOR-dependent mechanism of action for TRIM44, we have not proved the directionality of the interaction, i.e. whether TRIM44 activity is necessary for mTOR signaling, or vice-versa. Assuming that TRIM44 is a modulator of mTOR activity, our results cannot be used to ascertain its *exact* location within the mTOR pathway, though the decrease in the p-Akt/Akt ratio following TRIM44 knockout suggests that TRIM44 acts upstream of Akt and is indirectly associated with PDK1 (phosphoinositide-dependent kinase 1), the kinase responsible for phosphorylating Akt at Thr308 and leading to its full activation [80]. Though PDK1 is constitutively active in mammalian cells, its upstream interaction with PIP3 has been shown to increase Akt phosphorylation [81]. A logical next step would be to immunoprecipitate the PIP3/PDK1/Akt complex in TRIM44 knockdown cells and observe whether fewer complexes form or if association of molecules within the complex is weaker, supporting a role for TRIM44 in stabilizing this complex.

TRIM44 overexpression is another logical extension of this study – we would predict that TRIM44 OX cells would demonstrate increased mTOR signaling, Akt phosphorylation, and growth. TRIM44 could be acting through multiple pathways other than just the mTOR/Akt axis – multiple direct and indirect interactors for TRIM44 have been elucidated, including known cell growth regulators such as TP53 and CDKN1A (**Supplementary Figure 6**). Given the relative lack of knowledge surrounding TRIM44

and its cellular effects, an *in vitro* RNA-seq analysis of TRIM knockdown cells would be a feasible follow-up to our study in order to both confirm interactions such as those with TP53 and CDKN1A while also directing our attention to novel molecular pathways that could be connected to cancer. Chemical inhibitors of mTOR signaling, such as rapamycin and everolimus, can assist with the aforementioned analysis; it has previously been shown that treatment of TRIM44-overexpressing cell lines with everolimus significantly decreased cellular viability [77], but the effects of this inhibition at the molecular level were not studied – it would be interesting to see whether TRIM44 knockdown and mTOR inhibition produce similar expression profiles in an RNA-seq analysis to confirm TRIM44 acts in an mTOR-dependent manner.

Our *in vitro* model system, N2A cells, is another element of the study that could be improved upon – though TRIM44 shares homology across dogs, humans and mice, the use of a cancerous cell line can potentially be confounding, especially when looking for changes in cell growth, as cancer cells have altered cell growth programs and metabolism. An *in vivo* alternative would be to use mouse embryonic stem cells with the $Trim44^{tm1(KOMP)Vlcg}$ deletion allele (UC Davis) – this allele could be combined with a second mutation that induces brain cancer in order to test *in vivo* effects of TRIM44 on cancer growth.

The methodology used here to extract TRIM44 and distill it to its molecular functions in cell aging and cancer is one that we hope to continue cultivating using the strength of our FFPE canine brain dataset. The advantage of this analysis lies both in its abundance of samples and its superior homology to human aging compared to a majority of rival mammalian systems including mice. Though our functional analysis of

TRIM44 was not exhaustive, it is only a stepping stone in terms of longitudinal, aging-related information that can be extracted from RNA-seq analysis of canine brains. For example, out of hundreds of genes from the canine genome assembly (CanFam3.1) that we observed to have a significant difference in expression with age, a large portion of these genes were as-of-yet uncharacterized loci ("ENSCAFG" genes). In some cases, BLAST analysis of these loci yielded olfactory genes, which is expected given the evolution and amplification of canine olfactory receptor (OR) genes [83]. In the remaining cases, these ENSCAFG genes either a) had no homologs in humans, or b) were functionally unannotated genes. As described earlier, canines have the largest variability in adult lifespans of any mammalian species, so functional analysis of these ENSCAFG genes, which in many cases were both highly expressed and highly correlated with aging, offers an extremely promising avenue for discovering novel molecular markers of aging and its diseases.

Additionally, the brain tissues used in this study were only sampled from two breeds, Beagles and Boxers, which have relatively similar average lifespan (Beagle – 13.5yr, Boxer – 11, data from AKC). Differences in gene expression with age will likely be much more pronounced in a follow-up study using a more shorter-lived breed, such as St. Bernards or Great Danes. In the same vein, though Boxers do have highly increased susceptibility to intercranial neoplasias, certain breeds, such as the Cocker Spaniel, have been shown to be significantly *resistant* to the same types of brain tumors, making them a potentially more powerful control group than Beagles.

Lastly, our analysis was limited to only genes with *linear* correlations with aging, ignoring equally important genes with exponential or logarithm patterns of expression.

Genes associated with neurodevelopment in humans, for instance, have shown a flourish of different transcriptomic trajectories depending based on their cellular process [83], and a future direction of this study will be to analyze these genes are thoroughly as those with only linear correlations with age.

Some confounding factors to this analysis have been mentioned, but it is a fair commentary of the experimental design to critique the quality of RNA extracted from FFPE samples. Though addition of an rRNA-depletion step helps to increase mapping fidelity, it also significantly decreases total RNA yield, which in turn predisposes the sequencing libraries to PCR bias. This source of error cannot be solved simply by increasing the number of histological FFPE slices used to generate RNA, as this simultaneously increase the amount of DNA contamination in the sequencing libraries. Ignoring concerns of yield, the fixation process introduces genetic mutations through protein-RNA crosslinking, which excludes allelic variation from the scope of this study. This in turn masks aging-related genes that have gain/loss-of-function alleles in certain breeds. In many cases, single gene variations can trigger predisposition to diseases of aging, mutations in dog leukocyte antigen (DLA), for instance, increasing the risk of canine diabetes [84]. In this regard, this study could only detect transcriptome-level effects of aging. However, there is opportunity to use the Illumina CanineHD Whole-Genome Genotyping Beadchip in a follow-up study in order to connect breed-specific alleles with longevity, though this would require either higher quality RNA samples or a much larger sample size of FFPE samples in order to increase statistical power and filter out random mutations caused by the fixation process.

A final hurdle that this study seeks to overcome is proving that the genes whose expression correlates with age have clinical relevance – mammals undergo numerous non-pathological changes with age, not limited to loss of elasticity of the skin, loss of bone and muscle mass, and vision and hearing impairment [85]. Although interesting in their own respect, it is an obstacle faced by this study to zone in on genes that will be applicable to extension of life and prevention of aging-related disease, rather than genes responsible for secondary effects of aging. In the study presented here, GO term analysis helped prove that our dataset was indeed looking at genes related to disease of aging, highlighting cancer, nervous system development, and inflammatory disease as overrepresented categories (**Supplementary Figure 3**). It is also possible that the same upstream pathways that lead to sensory and skeletal degeneration with age are connected to those responsible for more serious conditions such as cancer and neurodegenerative disease; stem cell depletion or a shift to stem-cell differentiation rather than self-renewal, for example, could be the mechanism at work in both scenarios. To return to the previously-discussed “programmed aging” model, it is possible that diseases such as ALS and loss of skin elasticity with age can both be a result of cellular growth programs that remain overactive in late life, leading to deleterious side-effects, such as senescence-associated inflammation, in their respective tissue [86].

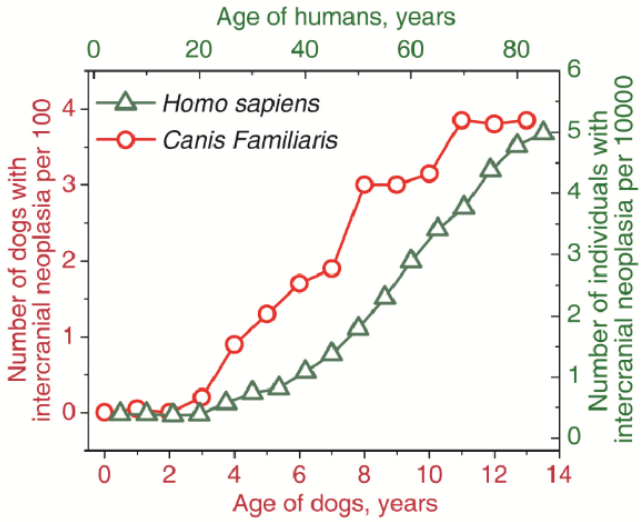

Figure 1. Incidence of brain cancers increases exponentially with age in both dogs and humans. Data from Song et al (dogs) [72] and 2013 NIH statistics (humans).

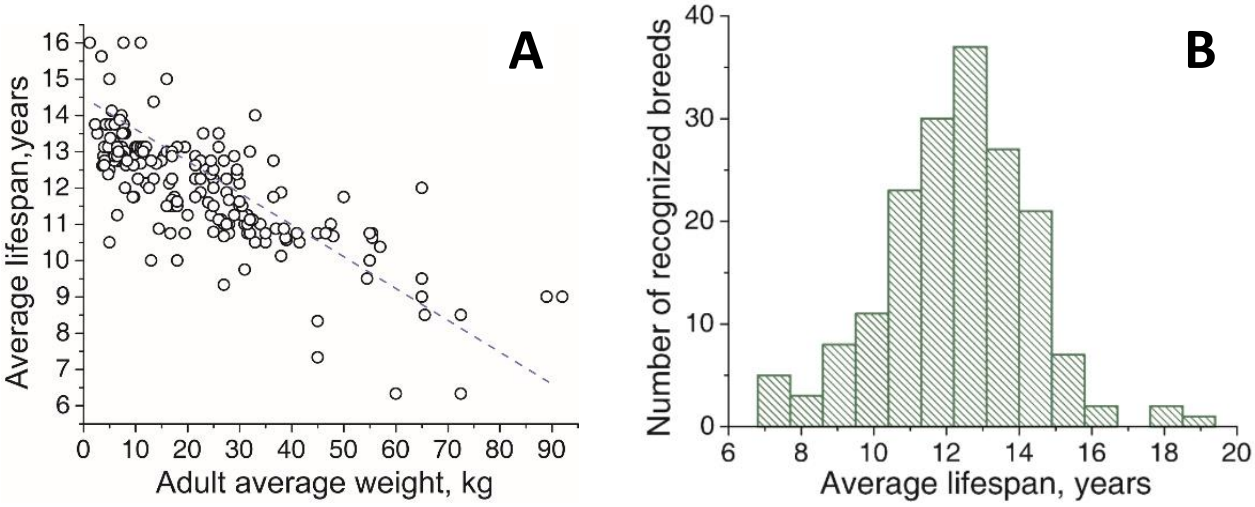

Figure 2. AKC weight and lifespan data for all recognized dog breeds. **A)** Average lifespan correlates negatively with average adult weight across all 178 AKC-recognized dog breeds. Each dot represents a unique breed. **B)** Distribution of lifespans across all 178 AKC breeds.

Table 1. Summary of processed FFPE canine brains

SAMPLE ID	BREED	GENDER	AGE(YR)	STATUS
07-94958-7	Beagle	Male	3	Intact
08-101092-5	Boxer	Female	7	Spayed
09-15348-4	Boxer	Female	2	Spayed
10-135448-ADD1	Boxer	Female	8	Spayed
11-11833-9	Beagle	Female	11	Spayed
12-106621-6	Beagle	Female	7	Spayed
13-83550-13	Beagle	Female	4	Intact
13-162213-11	Boxer	Male	11	Intact
07-128315-13	Boxer	Male	10	Castrate
11-20219-6	Boxer	Male	4	Castrate
11-54274-7	Boxer	Female	1	Spayed
12-114730-8	Boxer	Male	5	Castrate
12-113973-9	Beagle	Male	1	Intact
12-40718-ADD7	Beagle	Male	9	Intact
07-89459-4	Beagle	Male	6	Intact

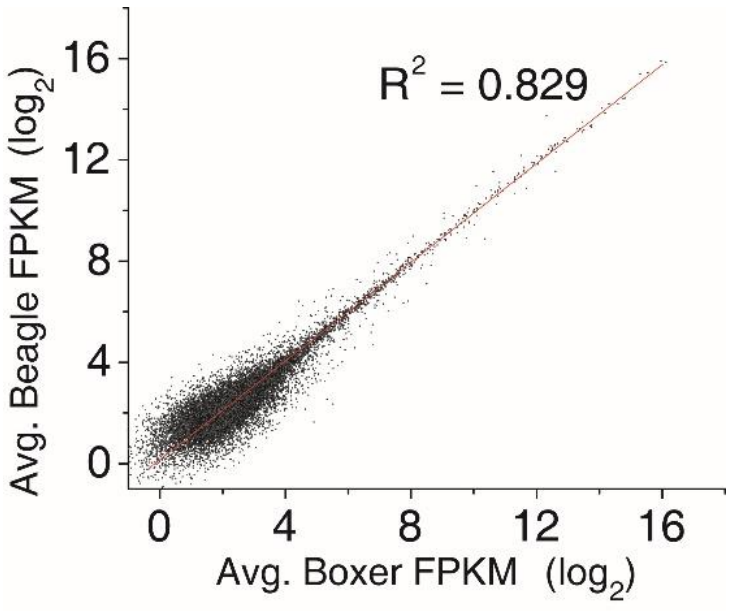

Figure 3. Correlation plot of average Beagle and Boxer gene expression (FPKM). Averaged 6-year and 7-year Beagle FPKM data was plotted over averaged 7-year Boxer and 8-year Boxer FPKM data. FPKM was calculated using cuffdiff. Each dot represents a single gene. Linear regression was fitted using the Deming regression model. High R^2 value indicates low variability/noise between similarly-aged samples.

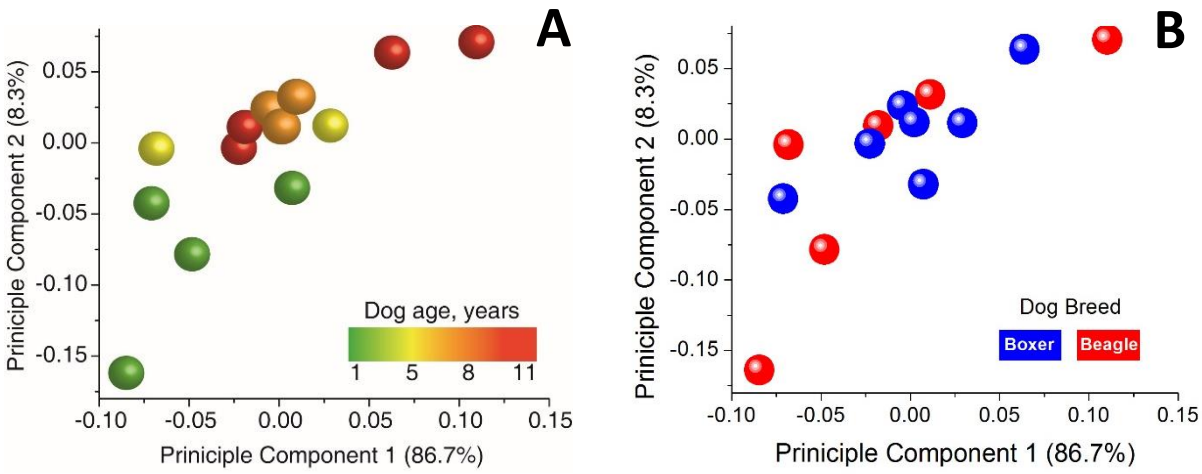

Figure 4. Principle component analysis of 15 canine cerebral cortex expression profiles. Principle components were calculated computationally from log2-normalized expression data using built-in packages in R. Each point consists of approximately 22,000 parameters (number of genes in the CanFam3.1 genome assembly with known transcript sequences). Note the clustering of points by age in **A)**, with a gradual transition from young to old samples, compared to the lack of clustering by breed in **B)**.

Table 2. Summary of co-directional gene overlap between human, dog, and mouse brain aging datasets

	rich 1		activity; zinc ion binding
FOSL1	FOS like antigen 1	Nucleus	RNA polymerase II core promoter proximal region sequence-specific DNA binding; sequence-specific DNA binding transcription factor activity
LRPPRC	leucine rich pentatricopeptide repeat containing	Cytoplasm	actin filament binding; beta-tubulin binding; microtubule binding; protein binding; RNA binding; single-stranded DNA binding; ubiquitin protein ligase binding
MMP23B	matrix metallopeptidase 23B	Extracellular Space	hydrolase activity; metal ion binding; metallopeptidase activity; peptidase activity; zinc ion binding
OLFM1	olfactomedin 1	Cytoplasm	beta-amyloid binding
RGS2	regulator of G-protein signaling 2	Nucleus	beta-tubulin binding; calmodulin binding; GTPase activator activity; protein binding
SFXN3	sideroflexin 3	Cytoplasm	ion transmembrane transporter activity; tricarboxylate secondary active transmembrane transporter activity
SLC9A3R1	solute carrier family 9, subfamily A (NHE3, cation proton antiporter 3), member 3 regulator 1	Plasma Membrane	beta-2 adrenergic receptor binding; beta-catenin binding; chloride channel regulator activity; dopamine receptor binding; growth factor receptor binding; PDZ domain binding; phosphatase binding;
TGIF2	TGFB-induced factor homeobox 2	Nucleus	DNA binding; sequence-specific DNA binding transcription factor activity
TRIM44	tripartite motif containing 44	Cytoplasm	metal ion binding; protein binding; zinc ion binding

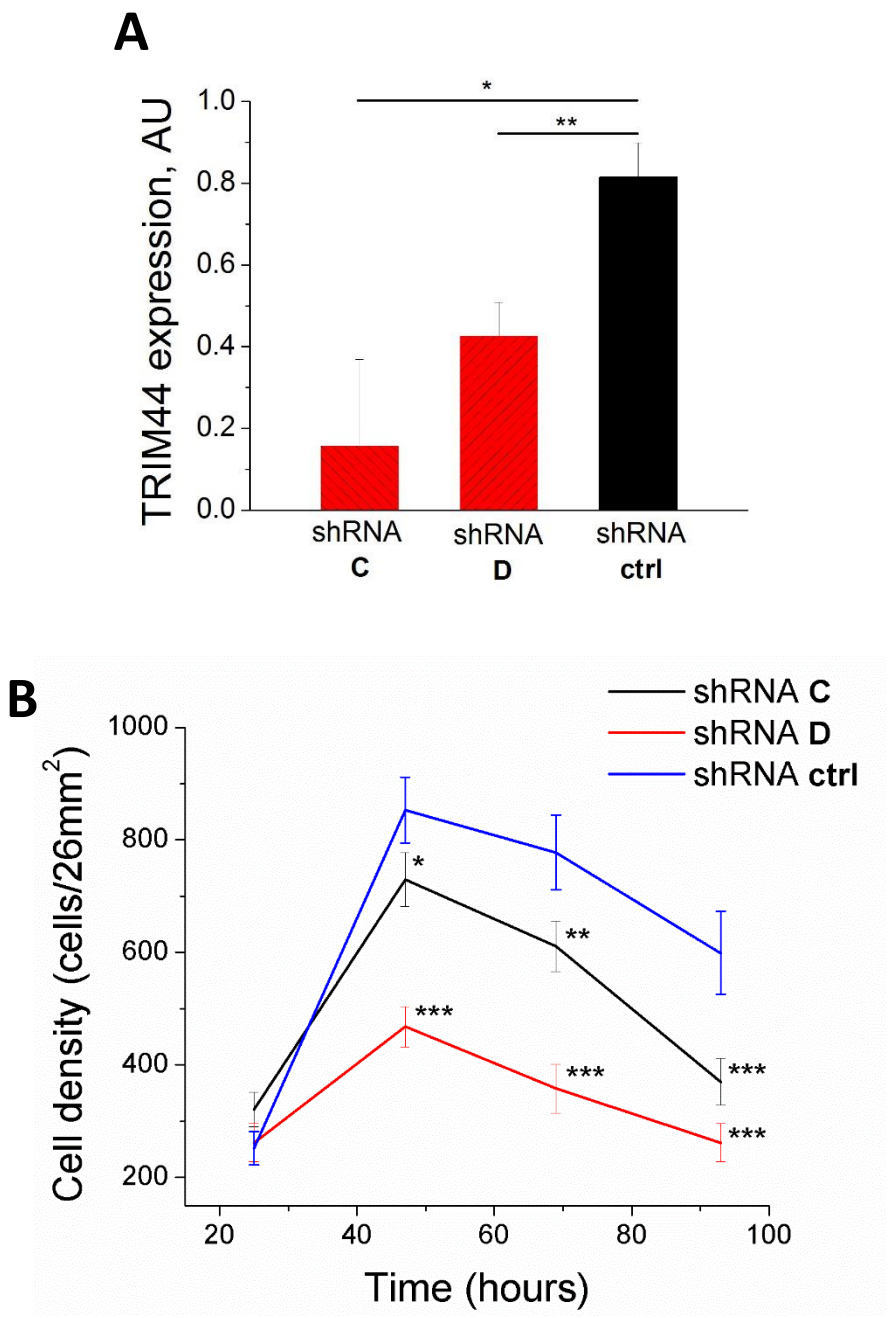

Figure 5. TRIM44 RNA knockout and cell density decrease in mTRIM44 shRNA-transfected N2A cells.
N2A cells were transiently transfected with different TRIM44 shRNA constructs (including scramble shRNA) and assayed for growth in a 6-well plate at various timepoints post-transfection. **A)** RNA levels where measured using qPCR at the last timepoint of the **B)** growth curve of the N2A transfectants, showing significant RNA-level knockdown. Growth curve error bars computed as S.E. of 35 technical repeats, qPCR as S.E of 3 technical repeats. Statistical significance calculated using Student's t-test, $P<0.5$ (*), $P<0.05$ (**), $P<0.005$(***).

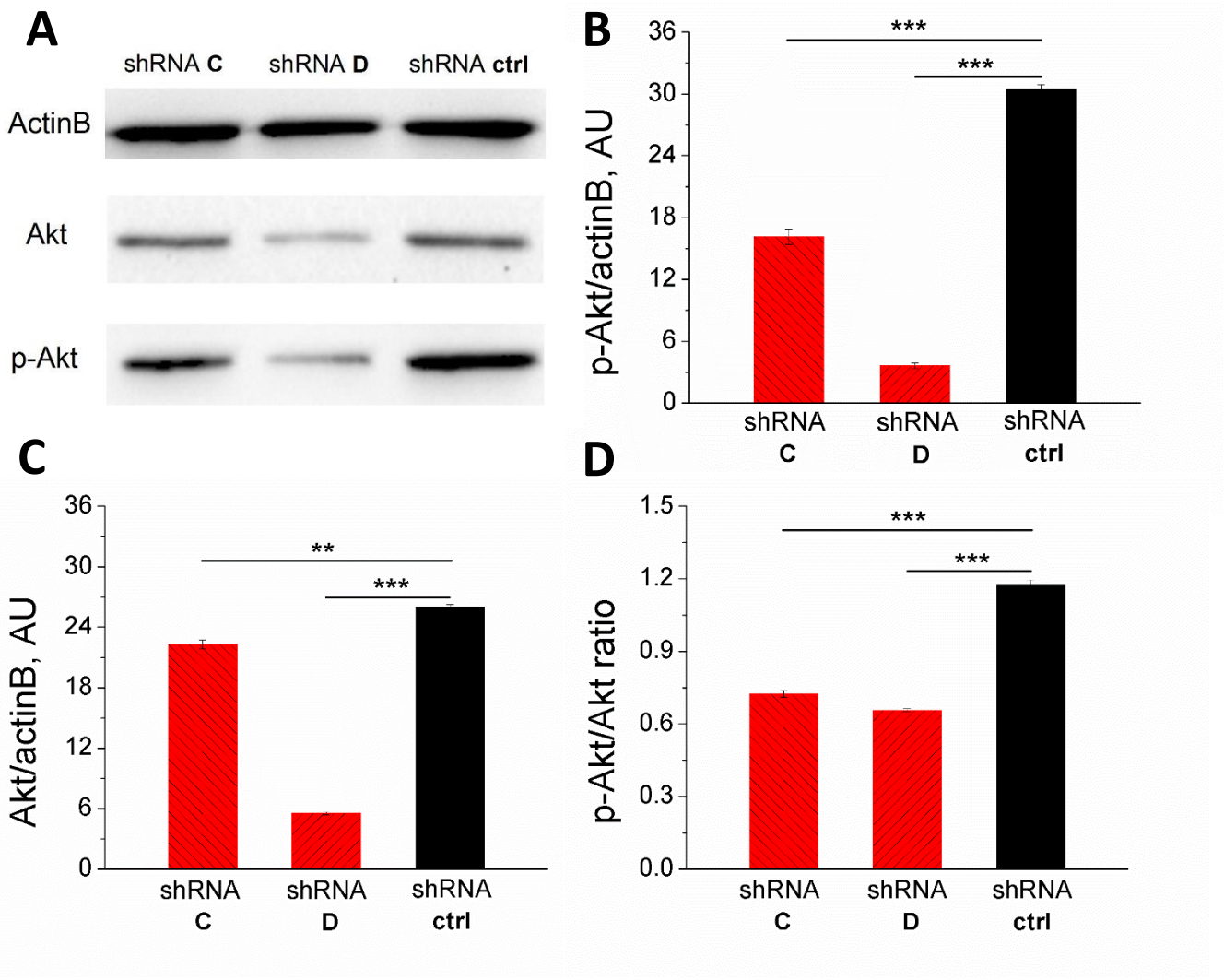

Figure 6. Protein-level quantification of p-Akt/Akt in TRIM44 shRNA-transfected N2A cells. Western blots were performed on lysates from N2A cells at 93hr post-transfection with TRIM44 shRNA constructs. Protein levels were normalized to ActinB expression.
Error bars computed as S.E. of 3 technical repeats. Statistical significance calculated using Student's t-test, P<0.5 (*), P<0.05 (**), P<0.005(***).

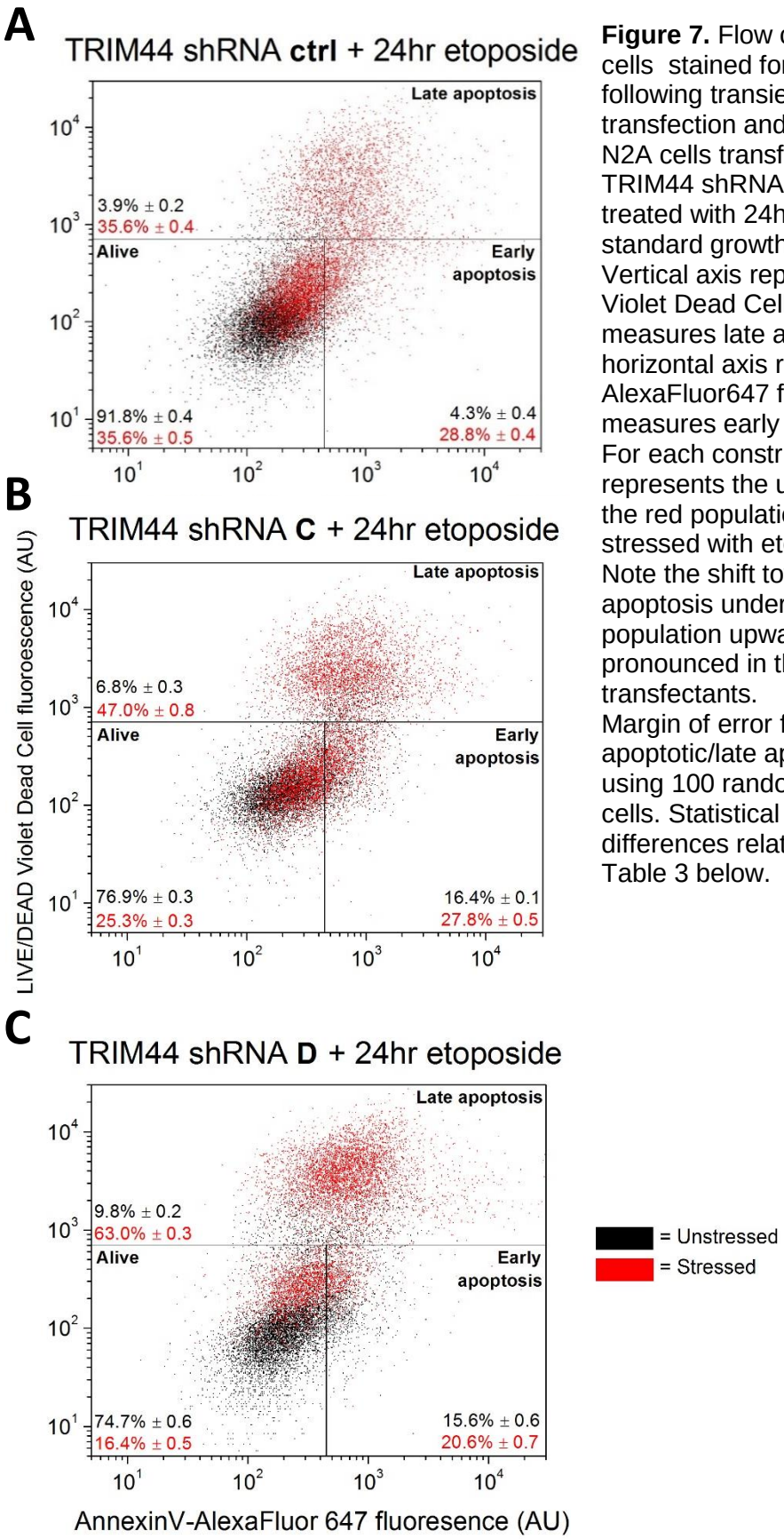

Figure 7. Flow cytometry analysis of N2A cells stained for apoptotic markers following transient TRIM44 shRNA transfection and etoposide stress.
N2A cells transfected with various TRIM44 shRNA constructs **(A-C)** were treated with 24hr of 100uM etoposide in standard growth media.
Vertical axis represents LIVE/DEAD Violet Dead Cell fluorescence, which measures late apoptosis, while the horizontal axis represents AnnexinV-AlexaFluor647 fluorescence, which measures early apoptosis.
For each construct, black population represents the unstressed sample, while the red population represents cells stressed with etoposide.
Note the shift towards increased late apoptosis under stress (shift of red population upwards), which is more pronounced in the non-control transfectants.
Margin of error for cell state (alive/early apoptotic/late apoptotic) were computed using 100 random samplings of 1000 cells. Statistical significance of population differences relative to the control are in Table 3 below.

Table 3. Summary of flow cytometry results of transiently TRIM44 shRNA-transfected N2A cells following etoposide stress

Key: $P<10^{-4}$ (***), $P<0.1$(*)			Percent of cells in given cell state		
			Alive	**Early apoptotic**	**Late apoptotic**
shRNA **ctrl** vs. shRNA **C**	No stress	shRNA **ctrl**	91.8	4.3	3.9
		shRNA **C**	76.9	16.4	6.8
		stat. sig.	****	****	****
	24hr etoposide	shRNA **ctrl**	35.6	28.8	35.6
		shRNA **C**	25.3	27.8	47.0
		stat. sig.	****	*	****
shRNA **ctrl** vs. shRNA **D**	No stress	shRNA **ctrl**	91.8	4.3	3.9
		shRNA **D**	74.7	15.6	9.8
		stat. sig.	****	****	****
	24hr etoposide	shRNA **ctrl**	35.6	28.8	35.6
		shRNA **D**	16.4	20.6	63.0
		stat. sig.	****	****	****

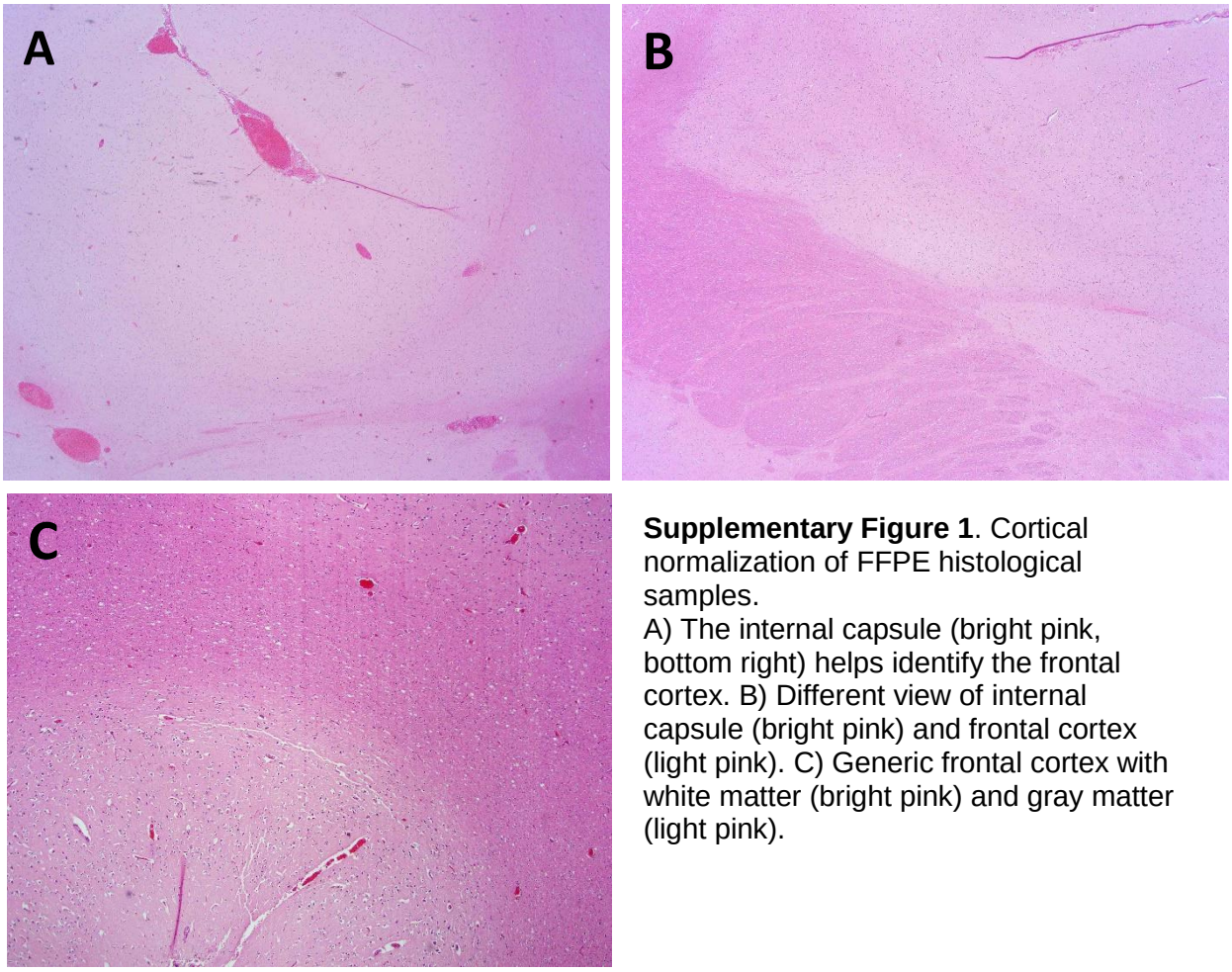

Supplementary Figure 1. Cortical normalization of FFPE histological samples.
A) The internal capsule (bright pink, bottom right) helps identify the frontal cortex. B) Different view of internal capsule (bright pink) and frontal cortex (light pink). C) Generic frontal cortex with white matter (bright pink) and gray matter (light pink).

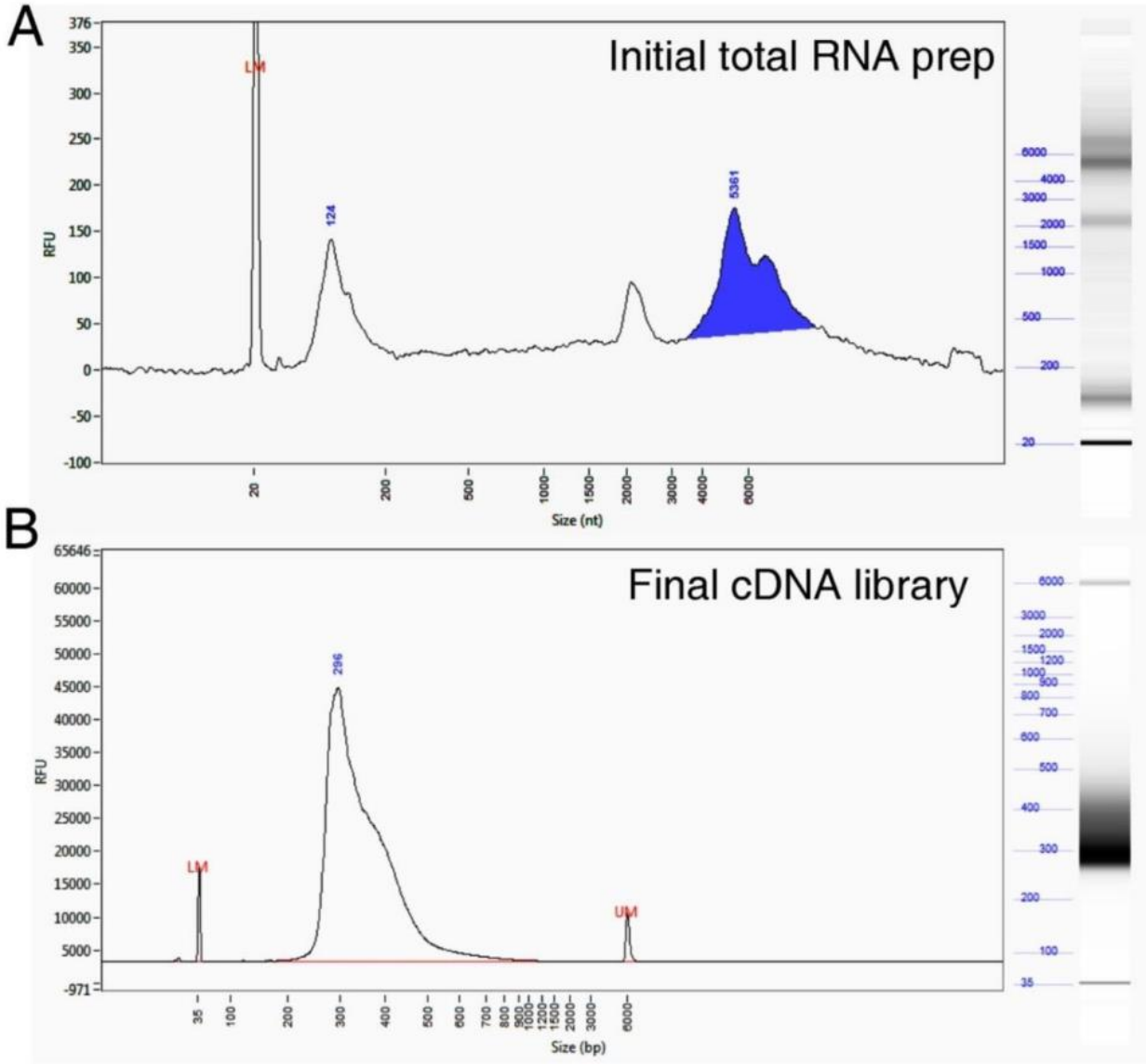

Supplementary Figure 2. Fragment analysis of canine RNA sequencing library from FFPE brain tissue.
A) Total RNA prep, with contamination of ribosomal RNA (blue) as well as other non-specific species. B) Final cDNA library – note the removal of large fragments as well as the homogenization of small bands into a single peak of relatively narrow fragment length distribution. The shift in primary peak size (124 before library preparation, 296 after) indicates successful sequencing adapter ligation.

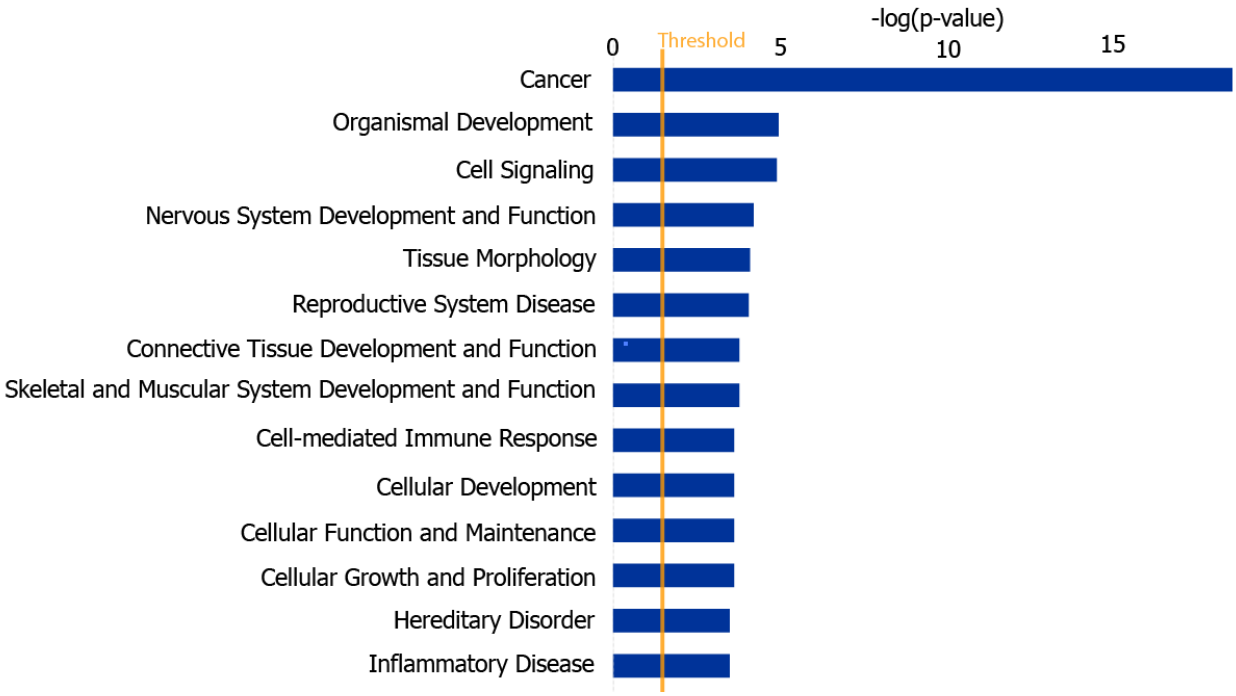

Supplementary Figure 3. GO analysis of genes with strong linear regression (R^2>0.5) with age.
GO analysis was performed using the QIAGEN Ingenuity Pathway Analysis software with raw FPKM values from 15 canine brain sequencing libraries. Threshold signifies a Bonferroni-corrected P-value cutoff of 0.05.

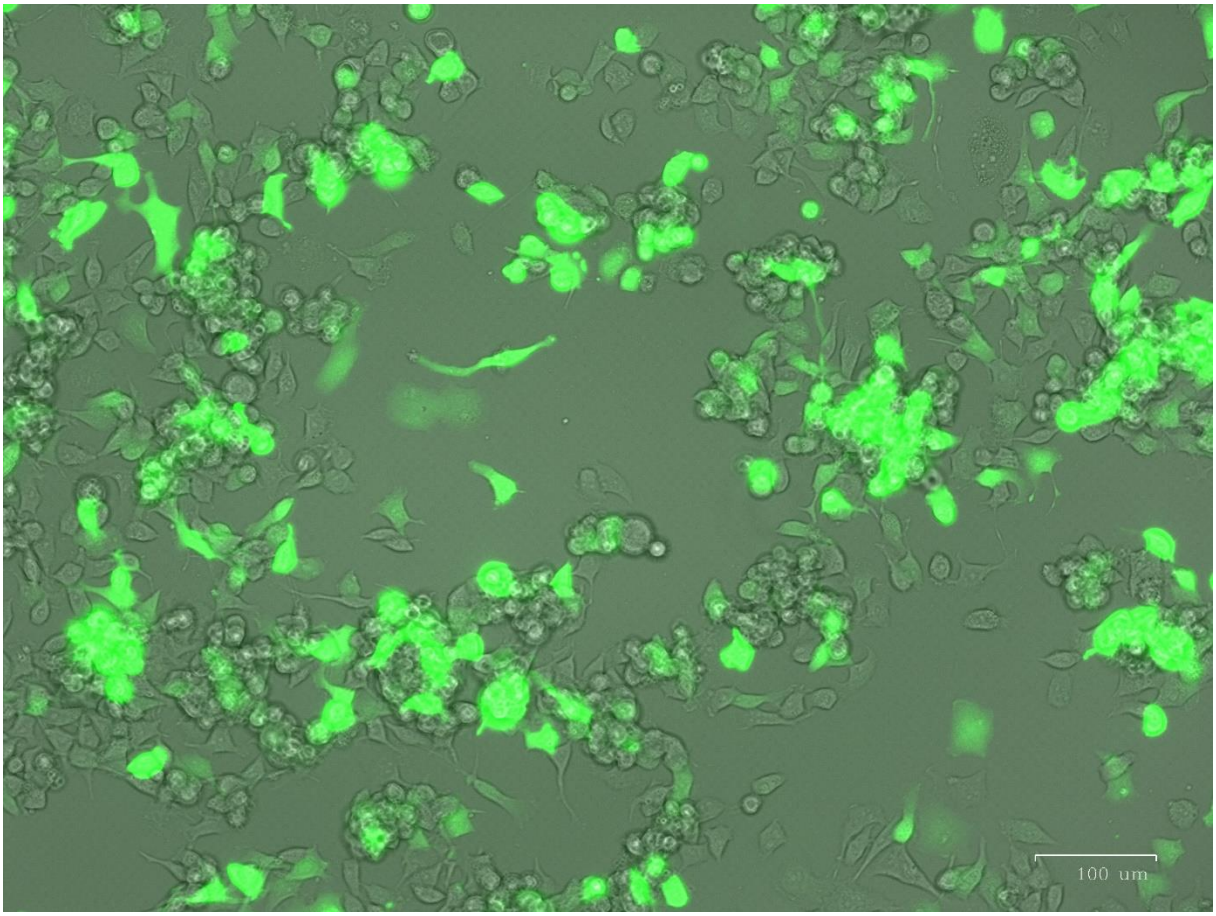

Supplementary Figure 4. Representative image of GFP expression of TRIM44 shRNA-transfected N2A cells at 47 hours post-transfection.
Cells were transiently transfected using a 1-to-7 ratio of ug plasmid DNA to FuGENE® HD Transfection Reagent. GFP is expressed from a tGFP gene under the control of a CMV promoter.

A

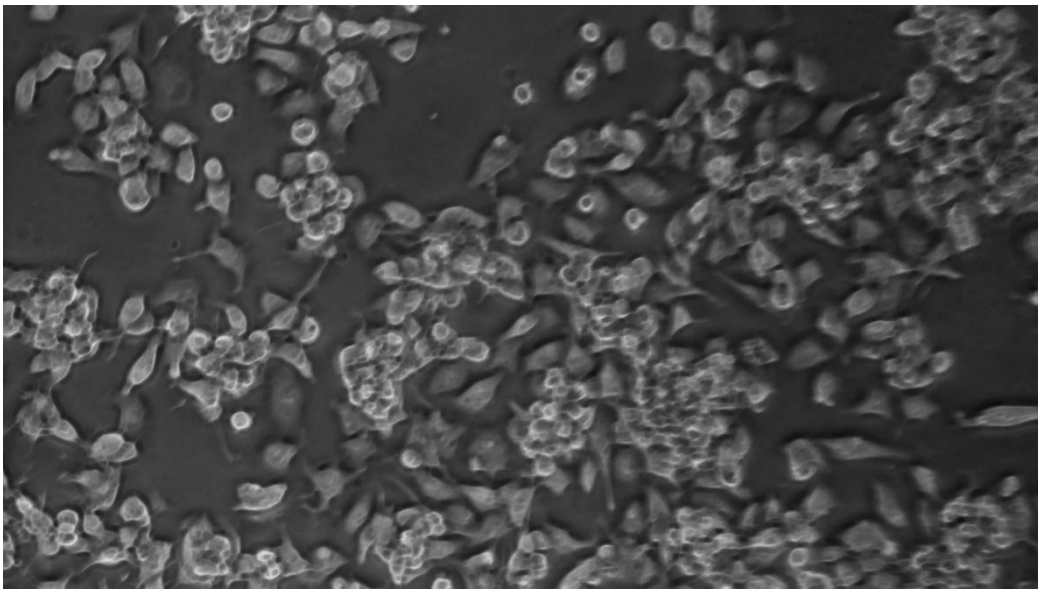

B

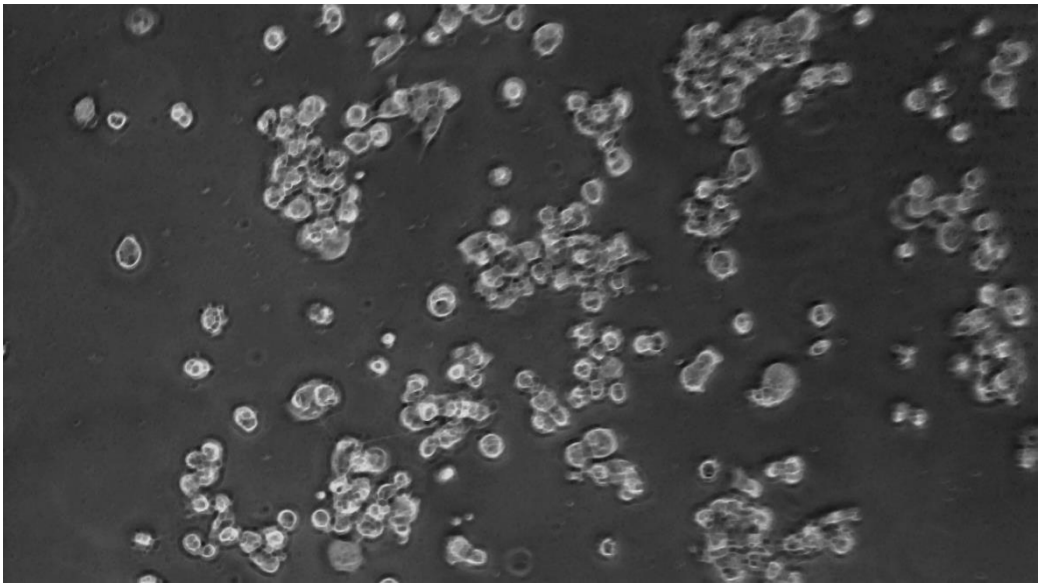

Supplementary Figure 5. N2A cell response to 24 hour of 100uM etoposide stress. A) Unstressed cells show markedly increased cell count, healthier shape (oblong, flat), and increased adhesion to the culture plate compared to B) cells treated with 24hr etoposide. Note the visible increase in dead (circular) cells in B).

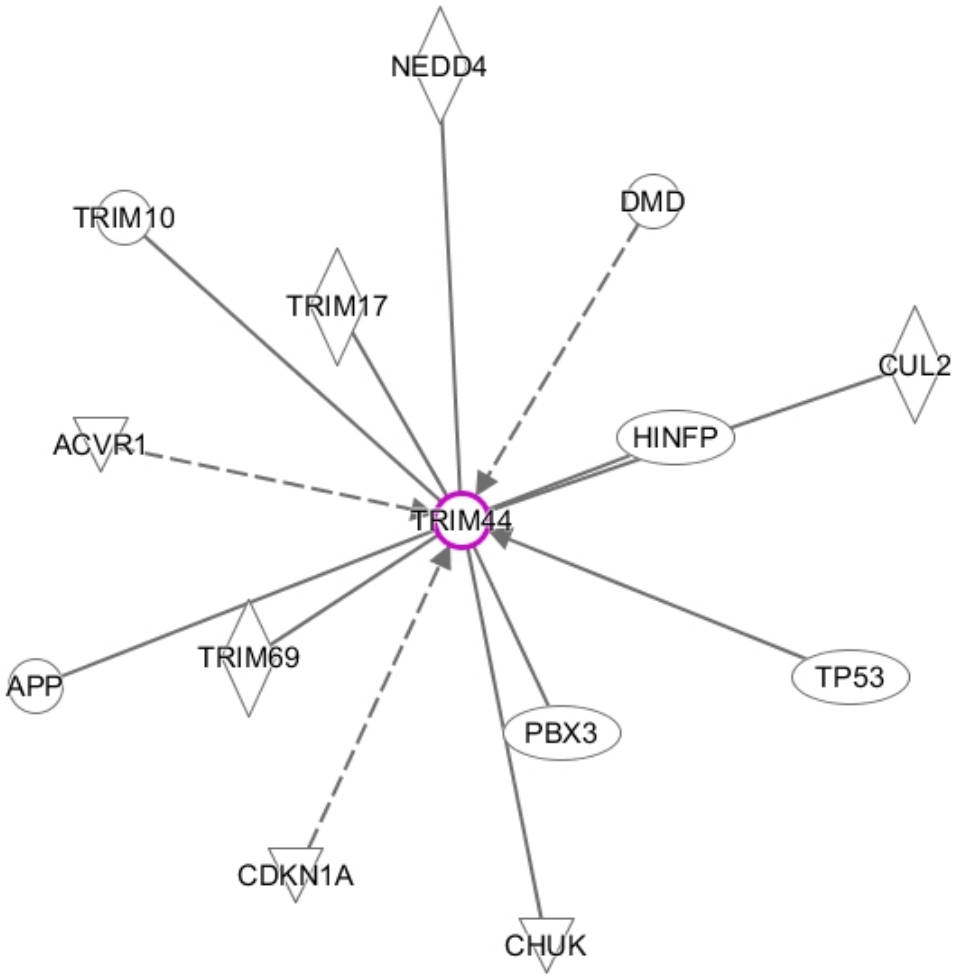

Supplementary Figure 6. Known molecular interactors of TRIM44.
Solid lines represent *direct* interactors (molecules that associate with TRIM44), while dotted lines represent *indirect* interactors. All observations are supported by at least one reference from the QIAGEN Ingenuity Pathway Analysis Knowledge Base.

ANIMAL HEALTH DIAGNOSTIC CENTER

Cornell University
240 Farrier Rd
ITHACA, NY 14853
Phone #: 607-253-3900 Fax #: 607-253-3943

Patient ID: 185260

Owner: GEOFF DIX

To: CORNELL UNIVERSITY HOSPITAL FOR ANIMAL
Attn: DR DIANE SCHREMPP
ITHACA, NY 14853

Phone # 607-253-3100

Accession Number: 94958-07
Reference Number: DIX, GEOFF
Case Coordinator:
Received: 07/23/2007 **Finalized:** 08/15/2007
Sampled: 07/21/2007

Case Summary

Species	Animals	Tests	Completed
CANINE	1	3	3

History: PATHOLOGY SERVICE REQUESTED: OWNER, BILL CLIENT-owner bill client
DIED/EUTHANIZED DIED-died
METHOD OF EUTHANASIA N/A - DIED-
DATE/TIME OF DEATH: -July 21, 2007, 5:30pm
HISTORY: -This is a healthy dog who has been healthy for all three years of its life. On Friday (7-20), in the evening he didn't want to eat and acted kinda dopey. On Saturday (7-21) AM, he was breathing shallow and heavy. He always had chip in a.m. when owner made lunch he didn't want anything. Saturday at noon he ate a scrambled egg but acted like he still wasn't there. By 3;30 he just layed by the owner's chair. At 5:30, the owners tried to get him to eat or drink but he looked up and convulsed and died.
HUSBANDRY (FEED,VACC,TRAVEL HX,NEW ADDITIONS): -The owners horse passed away just the same way as the dog (acting the same, not drinking, dopey) and the horse was diagnosed with EEE. They want to know if the dog has it so they know if they have problems in the area.
DURATION OF ILLNESS: -one day
PERTINENT CLINCIAL HISTORY: -see above, dog current on rabies and other vaccinations
CLINICAL DIAGNOSIS: -unknown
PRIVATE CREMATION: NO-group cremation

Final Report

ANATOMIC PATHOLOGY RESULTS

Section of Anatomic Pathology
Department of Biomedical Sciences
College of Veterinary Medicine
Ithaca, NY 14853

Necropsy Results:

ANIMAL ID	SPECIES	BREED	SEX	AGE
DOZER	Canine	Beagle Hound	Male	3y

Necropsy, Final

Patient ID: 185260

ANIMAL HEALTH DIAGNOSTIC CENTER
Cornell University
240 Farrier Rd
ITHACA, NY 14853
Phone #: 607-253-3900 Fax #: 607-253-3943

Final Report

Accession Number: 94958-07

Final Diagnosis

Dirofilariasis, vena caval syndrome

Final Comments

The histological findings support the suggestion that vena caval syndrome associated with severe heartworm (Dirofilaria immitis) infection was the cause of the death of this animal. There was no histologic evidence of Eastern Equine Encephalitis infection in this dog.

Measurements of the heart were taken at necropsy to quantify the changes associated with severe heartworm infection (see attachment). The increase in right ventricular weight when compared with both body and heart weight confirms right ventricular hypertrophy. The decreased aortic valve circumference compared with the pulmonic valve circumference and the increased pulmonic valve circumference compared with both the right and left atrioventricular valve circumference confirm the dilation of the pulmonary artery that was seen grossly.

Histologic Diagnosis

Heart: Severe chronic multifocal to coalescing myocarditis; Severe chronic locally extensive endoarteritis

Lung: Moderate diffuse chronic perivascular fibrosis and endoarteritis; Diffuse eosinophilic granulomatous interstitial pneumonia; Mild diffuse pulmonary edema

Kidney: Mild chronic cortical interstitial nephritis; Mild chronic membranous glomerulonephritis

Liver: Severe diffuse chronic centrilobular necrosis; Mild chronic periportal hepatitis

Spleen: Mild focal splenic necrosis; Splenic lymphoid depletion; Extramedullary hematopoiesis

All tissues: Myriad of intravascular microfilaria

Description

HEART: (Slide 1; 2 sections): The cardiac vessels are filled with microfilaria. The myocardial fibers are of varying size. There are multi-focal to coalescing areas of myocardial cell degeneration and necrosis associated with a mixed inflammatory infiltrate consisting mainly of macrophages with fewer lymphocytes, plasma cells, and neutrophils.

SPLEEN: (Slide 1; 1 section): Numerous microfilaria are present throughout vessels and interstitium. Throughout the white pulp there are multifocal to coalescing pale areas (depletion of lymphoid tissue). The red pulp has increased cellularity, associated with plasma cell infiltrate and focal areas of pyknotic debris and fibrin deposition (necrosis). Fibrin deposition is also occasionally present within red pulp

Patient ID: 185260

ANIMAL HEALTH DIAGNOSTIC CENTER
Cornell University
240 Farrier Rd
ITHACA, NY 14853
Phone #: 607-253-3900 Fax #: 607-253-3943

Final Report

Accession Number: 94958-07

capillaries (thrombi). Scattered throughout the red pulp parenchyma are megakaryocytes and pigment laden macrophages.

LIVER: (Slide 2 & 3; 6 sections): In all sections, the hepatic vessels and sinusoids contain numerous microfilaria. There is collapse of hepatic lobules due to hepatocellular loss within centrilobular areas. Within affected areas the hepatocytes have piknotic nuclei, cellular debris, and clusters of fibrin (necrosis). The periportal interstitium and lymphatics are dilated with pale pink staining homogenous material with peripheral dark pink droplets (edema) throughout, which is a mild mixed inflammatory cellular infiltrate.

LUNG: (Slide 3, 4 & 5; 6 sections): In 2 sections on slide 4 an alveolar blood vessel is obliterated by a large granuloma, which contains a cross section of a nematode with a cuticle, polymyarian, celomyarian musculature, and internal organs (Dirofilaria immitis). The lumen of most pulmonary capillaries and larger vessels contain numerous microfilaria. The alveolar lumen are flooded with pale eosinophilic homogenous material (edema). There are multifocal interstitial areas where the lung parenchyma is replaced by a mixed inflammatory cell infiltrate including macrophages, eosinophils, lymphocytes, and occasional multinucleate giant cells (eosinophilic granuloma). There are occasional alveolar macrophages with dark brown pigment (hemosiderin). There is perivascular fibrosis thoughout all sections and occasional small fibrin thrombi within the lumen of capillaries.

KIDNEY: (Slide 6; 1 section): Microfilaria are present within blood vessels in both the renal cortex and medulla. There is mild diffuse infiltration of inflammatory cells into the cortical interstitium (interstitial nephritis). There is mild to moderate segmental thickening of the glomerular basement membrane with a pale eosinophilic globular deposits (membranous glomerulonephritis). Within the lumen of renal tubules are small clusters of orange pigment (hemoglobin). Numerous tubular epithelial cells and macrophages contain a dark brown pigment (hemosiderin). A single fibrin thrombus is present in a glomerular capillary.

BRAIN, NOS: (Slide 7; 1 section): No abnormalities detected.

Pathologist Dr. Gerald Duhamel
Resident Pathologist Dr. Elizabeth Dobson

Necropsy, Gross

Patient ID: 185260

ANIMAL HEALTH DIAGNOSTIC CENTER
Cornell University
240 Farrier Rd
ITHACA, NY 14853
Phone #: 607-253-3900 Fax #: 607-253-3943

Final Report

Accession Number: 94958-07

FINDINGS

Heart, Lungs, Pulmonary Artery, Caudal Vena Cava:
Chronic, locally extensive, severe pulmonary verminous arteritis and phlebitis (Dirofilaria immitis)
Liver: Chronic, diffuse, passive congestion and fibrosis
Bladder: Diffuse multifocal petechiations; acute diffuse moderate cystitis

DIAGNOSIS

Dirofilariasis with secondary hepatic passive congestion

Gross Comments

The gross pathological findings are of severe heartworm disease (Dirofilaria immitis). The acuteness of this animal's clinical disease is consistent with caudal vena caval syndrome which is a complication of chronic, severe heartworm disease. Classically this syndrome is characterized by acute anorexia, respiratory distress, weakness, right-sided cardiac murmur, anemia, hepatic and renal dysfunction, heart failure and possibly disseminated intravascular coagulation (DIC). Shock occurs as a consequence of vascular occlusion and decreased venous return. The presence of adult heartworms in the right ventricle, right atrium and vena cavae leads to valvular insufficiency which, in combination with pulmonary hypertension, results in heart failure. In this case, passive congestion of the liver is the only gross finding consistent with heart failure. The presence of a large mass of worms within the vessels is traumatic to erythrocytes causing intravascular hemolysis. Intravascular hemolysis is the likely cause of the hemoglobinuria seen in this case.

Appropriate samples have been submitted for histopathology.

Description

This is the carcass of a 3 year old, 12.3 kg, intact male, brown and white beagle dog in good body condition with moderate autolysis. There are 3 petechia on the caudal aspect of the scrotum over the left testicle. The perineum is stained brown (fecal staining) and the caudoventral abdomen and left hind limb are stained yellow-green (urine staining). The subcutaneous, abdominal, and mesenteric fat is diffusely light yellow (icterus).

The pericardium contains approximately 3 ml of serosanguinous fluid. Throughout the caudal vena cava, right atrium, right ventricle, and pulmonary arteries are over a hundred white nematodes, often with corkscrew ends, between 15 and 30 cm long (adult Dirofilaria immitis (heartworms)). The pulmonary artery is dilated with "shaggy" thickening of the intima most prominent at the bifurcation. The left atrium and ventricle have 3 heartworms and dozens of dark red thin worm-like strands in a dark red gelatinous cast(blood clot with immature or dead adult heartworms).

Patient ID: 185260

ANIMAL HEALTH DIAGNOSTIC CENTER
Cornell University
240 Farrier Rd
ITHACA, NY 14853
Phone #: 607-253-3900 Fax #: 607-253-3943

Final Report

Accession Number: 94958-07

The pulmonary vessels over 0.2 cm in diameter contain 1 to 10 adult heartworms. The caudodorsal portion of lungs are shiny, rubbery and rib impressions are visible over the dorsal surface of all lobes (pulmonary edema). The right caudodorsal lung field is diffusely dark red and firm (congestion), and the left lobes have multifocal red areas ranging from 0.1 to 0.3 cm in diameter (hemorrhage). The caudal border of the left cranial lung lobe has a 1cm x 1cm x 0.5cm pale white, firm nodule which is attached to the pericardium with a fibrin tag. On cut section the nodule contains dead adult heartworms.

The liver is diffusely pale brown and firm with a mottled enhanced reticular pattern (chronic passive congestion). The reticular pattern is more prominent throughout the right lateral lobe which is more firm and has coalescing areas of parenchymal collapse fibrosis (presumptive).

The bladder contains approximately 5 mL of red viscous liquid and there is multifocal petechia throughout the mucosa (hemoglobinuria, cystitis). There is a 2 cm circumferential band of hyperemia in the stomach located 5 cm proximal to the pylorus and a 9 cm segment of hyperemia in the proximal colon.

Pathologist	Dr. Gerald Duhamel
Resident Pathologist	Dr. Elizabeth Dobson
Student	Stacy Choczynski

VIROLOGY RESULTS

Virus Isolation 15-AUG-07

ANIMAL ITEM	ANIMAL ID	SPECIES
1	DOZER	Canine

RESULT No Virus Isolated

West Nile Virus PCR 27-JUL-07

ANIMAL ITEM	ANIMAL ID	SPECIES	SPECIMEN DESC	Result
1	DOZER	Canine	Brain, Nos	Negative

Patient ID: 185260

ANIMAL HEALTH DIAGNOSTIC CENTER
Cornell University
240 Farrier Rd
ITHACA, NY 14853
Phone #: 607-253-3900 Fax #: 607-253-3943

Final Report

Accession Number: 94958-07

References

1. Niccoli, T. and L. Partridge (2012). "Ageing as a risk factor for disease." Curr Biol **22**(17): R741-752.
2. Signer, R. A. and S. J. Morrison (2013). "Mechanisms that regulate stem cell aging and life span." Cell Stem Cell **12**(2): 152-165.
3. Espada, J., I. Varela, et al. (2008). "Nuclear envelope defects cause stem cell dysfunction in premature-aging mice." J Cell Biol **181**(1): 27-35.
4. Lopez-Otin, C., M. A. Blasco, et al. (2013). "The hallmarks of aging." Cell **153**(6): 1194-1217.
5. Mostoslavsky, R., K. F. Chua, et al. (2006). "Genomic instability and aging-like phenotype in the absence of mammalian SIRT6." Cell **124**(2): 315-329.
6. Gorbunova, V., C. Hine, et al. (2012). "Cancer resistance in the blind mole rat is mediated by concerted necrotic cell death mechanism." Proc Natl Acad Sci U S A **109**(47): 19392-19396.
7. Zhao, S., L. Lin, et al. (2014). "High autophagy in the naked mole rat may play a significant role in maintaining good health." Cell Physiol Biochem **33**(2): 321-332.
8. Blagosklonny, M. V. (2012). "Cell cycle arrest is not yet senescence, which is not just cell cycle arrest: terminology for TOR-driven aging." Aging (Albany NY) **4**(3): 159-165.
9. Blagosklonny, M. V. (2013). "Hypoxia, MTOR and autophagy: converging on senescence or quiescence." Autophagy **9**(2): 260-262.
10. Skulachev, V. P. (2002). "Programmed death phenomena: from organelle to organism." Ann N Y Acad Sci **959**: 214-237.
11. Shay, J. W. and W. E. Wright (2000). "Hayflick, his limit, and cellular ageing." Nat Rev Mol Cell Biol **1**(1): 72-76.
12. Ackerman, D. and D. Gems (2012). "The mystery of C. elegans aging: an emerging role for fat. Distant parallels between C. elegans aging and metabolic syndrome?" Bioessays **34**(6): 466-471.
13. Kirkwood, T. B. (1977). "Evolution of ageing." Nature **270**(5635): 301-304.
14. Carter, A. J. and A. Q. Nguyen (2011). "Antagonistic pleiotropy as a widespread mechanism for the maintenance of polymorphic disease alleles." BMC Med Genet **12**: 160.
15. Horvath, S. (2013). "DNA methylation age of human tissues and cell types." Genome Biol **14**(10): R115.
16. Morris, B. J., D. C. Willcox, et al. (2015). "FOXO3: A Major Gene for Human Longevity--A Mini-Review." Gerontology **61**(6): 515-525.
17. Webb, A. E. and A. Brunet (2014). "FOXO transcription factors: key regulators of cellular quality control." Trends Biochem Sci **39**(4): 159-169.
18. Guarente, L. (2007). "Sirtuins in aging and disease." Cold Spring Harb Symp Quant Biol **72**: 483-488.
19. Morris, B. J. (2013). "Seven sirtuins for seven deadly diseases of aging." Free Radic Biol Med **56**: 133-171.
20. Chen, D., J. Bruno, et al. (2008). "Tissue-specific regulation of SIRT1 by calorie restriction." Genes Dev **22**(13): 1753-1757.
21. Weindruch, R. (1996). "The retardation of aging by caloric restriction: studies in rodents and primates." Toxicol Pathol **24**(6): 742-745.
22. Weindruch, R., R. L. Walford, et al. (1986). "The retardation of aging in mice by dietary restriction: longevity, cancer, immunity and lifetime energy intake." J Nutr **116**(4): 641-654.
23. Colman, R. J., T. M. Beasley, et al. (2014). "Caloric restriction reduces age-related and all-cause mortality in rhesus monkeys." Nat Commun **5**: 3557.
24. Colman, R. J., R. M. Anderson, et al. (2009). "Caloric restriction delays disease onset and mortality in rhesus monkeys." Science **325**(5937): 201-204.
25. Mattison, J. A., G. S. Roth, et al. (2012). "Impact of caloric restriction on health and survival in rhesus monkeys from the NIA study." Nature 489(7415): 318-321.

26. Colman, R. J., T. M. Beasley, et al. (2014). "Caloric restriction reduces age-related and all-cause mortality in rhesus monkeys." Nat Commun 5: 3557.
27. Duffy, P. H., J. E. Seng, et al. (2001). "The effects of different levels of dietary restriction on aging and survival in the Sprague-Dawley rat: implications for chronic studies." Aging (Milano) **13**(4): 263-272.
28. Liu, T., H. Qi, et al. (2015). "Resveratrol Attenuates Oxidative Stress and Extends Life Span in the Annual Fish Nothobranchius guentheri." Rejuvenation Res **18**(3): 225-233.
29. Baur, J. A., K. J. Pearson, et al. (2006). "Resveratrol improves health and survival of mice on a high-calorie diet." Nature **444**(7117): 337-342.
30. Mitchell, S. J., A. Martin-Montalvo, et al. (2014). "The SIRT1 activator SRT1720 extends lifespan and improves health of mice fed a standard diet." Cell Rep **6**(5): 836-843.
31. Herrington, J., L. S. Smit, et al. (2000). "The role of STAT proteins in growth hormone signaling." Oncogene **19**(21): 2585-2597.
32. Binder, G. (2009). "Noonan syndrome, the Ras-MAPK signalling pathway and short stature." Horm Res **71 Suppl 2**: 64-70.
33. Sutter, N. B., C. D. Bustamante, et al. (2007). "A single IGF1 allele is a major determinant of small size in dogs." Science **316**(5821): 112-115.
34. Subbarayan, S. K., M. Fleseriu, et al. (2012). "Serum IGF-1 in the diagnosis of acromegaly and the profile of patients with elevated IGF-1 but normal glucose-suppressed growth hormone." Endocr Pract **18**(6): 817-825.
35. Dorman, J. B., B. Albinder, et al. (1995). "The age-1 and daf-2 genes function in a common pathway to control the lifespan of Caenorhabditis elegans." Genetics **141**(4): 1399-1406.
36. Bartke, A. and H. Brown-Borg (2004). "Life extension in the dwarf mouse." Curr Top Dev Biol **63**: 189-225.
37. Guevara-Aguirre, J., P. Balasubramanian, et al. (2011). "Growth hormone receptor deficiency is associated with a major reduction in pro-aging signaling, cancer, and diabetes in humans." Sci Transl Med **3**(70): 70ra13.
38. Hinkal, G. and L. A. Donehower (2008). "How does suppression of IGF-1 signaling by DNA damage affect aging and longevity?" Mech Ageing Dev **129**(5): 243-253.
39. Nagano, I., M. Shiote, et al. (2005). "Beneficial effects of intrathecal IGF-1 administration in patients with amyotrophic lateral sclerosis." Neurol Res **27**(7): 768-772.
40. Al-Regaiey, K. A., M. M. Masternak, et al. (2005). "Long-lived growth hormone receptor knockout mice: interaction of reduced insulin-like growth factor i/insulin signaling and caloric restriction." Endocrinology **146**(2): 851-860.
41. Chistiakov, D. A., I. A. Sobenin, et al. (2014). "Mitochondrial aging and age-related dysfunction of mitochondria." Biomed Res Int **2014**: 238463.
42. Murphy, M. P. (2009). "How mitochondria produce reactive oxygen species." Biochem J **417**(1): 1-13.
43. Keyer, K., A. S. Gort, et al. (1995). "Superoxide and the production of oxidative DNA damage." J Bacteriol **177**(23): 6782-6790.
44. Barber, S. C., R. J. Mead, et al. (2006). "Oxidative stress in ALS: a mechanism of neurodegeneration and a therapeutic target." Biochim Biophys Acta **1762**(11-12): 1051-1067.
45. Kenyon, C. (2005). "The plasticity of aging: insights from long-lived mutants." Cell **120**(4): 449-460.
46. Hesp, K., G. Smant, et al. (2015). "Caenorhabditis elegans DAF-16/FOXO transcription factor and its mammalian homologs associate with age-related disease." Exp Gerontol **72**: 1-7.
47. Schulz, T. J., K. Zarse, et al. (2007). "Glucose restriction extends Caenorhabditis elegans life span by inducing mitochondrial respiration and increasing oxidative stress." Cell Metab **6**(4): 280-293.
48. Yalcin, S., D. Marinkovic, et al. (2010). "ROS-mediated amplification of AKT/mTOR signalling pathway leads to myeloproliferative syndrome in Foxo3(-/-) mice." EMBO J **29**(24): 4118-4131.

49. Bruns, D. R., J. C. Drake, et al. (2015). "Nrf2 Signaling and the Slowed Aging Phenotype: Evidence from Long-Lived Models." Oxid Med Cell Longev **2015**: 732596.
50. Redman, L. M. and E. Ravussin (2011). "Caloric restriction in humans: impact on physiological, psychological, and behavioral outcomes." Antioxid Redox Signal **14**(2): 275-287.
51. Tome-Carneiro, J., M. Larrosa, et al. (2013). "Resveratrol and clinical trials: the crossroad from in vitro studies to human evidence." Curr Pharm Des **19**(34): 6064-6093.
52. Gorbunova, V., A. Seluanov, et al. (2014). "Comparative genetics of longevity and cancer: insights from long-lived rodents." Nat Rev Genet **15**(8): 531-540.
53. Calado, R. T. and B. Dumitriu (2013). "Telomere dynamics in mice and humans." Semin Hematol **50**(2): 165-174.
54. MacRae, S. L., M. M. Croken, et al. (2015). "DNA repair in species with extreme lifespan differences." Aging (Albany NY) **7**(12): 1171-1184.
55. Seim, I., S. Ma, et al. (2014). "The transcriptome of the bowhead whale Balaena mysticetus reveals adaptations of the longest-lived mammal." Aging (Albany NY) **6**(10): 879-899.
56. Patrick, A., M. Seluanov, et al. (2016). "Sensitivity of primary fibroblasts in culture to atmospheric oxygen does not correlate with species lifespan." Aging (Albany NY) **8**(5): 841-847.
57. Li, Y. and J. P. de Magalhaes (2013). "Accelerated protein evolution analysis reveals genes and pathways associated with the evolution of mammalian longevity." Age (Dordr) **35**(2): 301-314.
58. Suh, Y., G. Atzmon, et al. (2008). "Functionally significant insulin-like growth factor I receptor mutations in centenarians." Proc Natl Acad Sci U S A **105**(9): 3438-3442.
59. Atzmon, G., M. Cho, et al. (2010). "Evolution in health and medicine Sackler colloquium: Genetic variation in human telomerase is associated with telomere length in Ashkenazi centenarians." Proc Natl Acad Sci U S A **107 Suppl 1**: 1710-1717.
60. Morris, B. J., T. A. Donlon, et al. (2015). "Genetic analysis of TOR complex gene variation with human longevity: a nested case-control study of American men of Japanese ancestry." J Gerontol A Biol Sci Med Sci **70**(2): 133-142.
61. Yuan, R., S. W. Tsaih, et al. (2009). "Aging in inbred strains of mice: study design and interim report on median lifespans and circulating IGF1 levels." Aging Cell **8**(3): 277-287.
62. Fan, Z., P. Silva, et al. (2016). "Worldwide patterns of genomic variation and admixture in gray wolves." Genome Res **26**(2): 163-173.
63. Perry, G. H., N. J. Dominy, et al. (2007). "Diet and the evolution of human amylase gene copy number variation." Nat Genet **39**(10): 1256-1260.
64. Axelsson, E., A. Ratnakumar, et al. (2013). "The genomic signature of dog domestication reveals adaptation to a starch-rich diet." Nature **495**(7441): 360-364.
65. Freedman, A. H., I. Gronau, et al. (2014). "Genome sequencing highlights the dynamic early history of dogs." PLoS Genet **10**(1): e1004016.
66. Wang, G. D., W. Zhai, et al. (2013). "The genomics of selection in dogs and the parallel evolution between dogs and humans." Nat Commun **4**: 1860.
67. Head, E. (2013). "A canine model of human aging and Alzheimer's disease." Biochim Biophys Acta **1832**(9): 1384-1389.
68. Selman, C., D. H. Nussey, et al. (2013). "Ageing: it's a dog's life." Curr Biol **23**(10): R451-453.
69. Speakman, J. R. (2005). "Body size, energy metabolism and lifespan." J Exp Biol **208**(Pt 9): 1717-1730.
70. von Ahlfen, S., A. Missel, et al. (2007). "Determinants of RNA quality from FFPE samples." PLoS One **2**(12): e1261.
71. Nowakowski, R. S. (2006). "Stable neuron numbers from cradle to grave." Proc Natl Acad Sci U S A **103**(33): 12219-12220.
72. Song, R. B., C. H. Vite, et al. (2013). "Postmortem evaluation of 435 cases of intracranial neoplasia in

dogs and relationship of neoplasm with breed, age, and body weight." J Vet Intern Med 27(5): 1143-1152.
73. Zahn, J. M., S. Poosala, et al. (2007). "AGEMAP: a gene expression database for aging in mice." PLoS Genet **3**(11): e201.
74. Boutou, E., R. Matsas, et al. (2001). "Isolation of a mouse brain cDNA expressed in developing neuroblasts and mature neurons." Brain Res Mol Brain Res **86**(1-2): 153-167.
75. Hatakeyama, S. (2011). "TRIM proteins and cancer." Nat Rev Cancer **11**(11): 792-804.
76. Napolitano, L. M. and G. Meroni (2012). "TRIM family: Pleiotropy and diversification through homomultimer and heteromultimer formation." IUBMB Life **64**(1): 64-71.
77. Ong, C. A., N. B. Shannon, et al. (2014). "Amplification of TRIM44: pairing a prognostic target with potential therapeutic strategy." J Natl Cancer Inst **106**(5).
78. Abbas, T. and A. Dutta (2009). "p21 in cancer: intricate networks and multiple activities." Nat Rev Cancer **9**(6): 400-414.
79. Pazarentzos, E. and T. G. Bivona (2015). "Adaptive stress signaling in targeted cancer therapy resistance." Oncogene **34**(45): 5599-5606.
80. Alessi, D. R., S. R. James, et al. (1997). "Characterization of a 3-phosphoinositide-dependent protein kinase which phosphorylates and activates protein kinase Balpha." Curr Biol **7**(4): 261-269.
81. Mora, A., D. Komander, et al. (2004). "PDK1, the master regulator of AGC kinase signal transduction." Semin Cell Dev Biol **15**(2): 161-170.
82. Niimura, Y. and M. Nei (2007). "Extensive gains and losses of olfactory receptor genes in mammalian evolution." PLoS One **2**(8): e708.
83. Kang, H. J., Y. I. Kawasawa, et al. (2011). "Spatio-temporal transcriptome of the human brain." Nature **478**(7370): 483-489.
84. Kennedy, L. J., L. J. Davison, et al. (2006). "Identification of susceptibility and protective major histocompatibility complex haplotypes in canine diabetes mellitus." Tissue Antigens **68**(6): 467-476.
85. Tosato, M., V. Zamboni, et al. (2007). "The aging process and potential interventions to extend life expectancy." Clin Interv Aging **2**(3): 401-412.
86. Coppe, J. P., P. Y. Desprez, et al. (2010). "The senescence-associated secretory phenotype: the dark side of tumor suppression." Annu Rev Pathol **5**: 99-118.